

Electronic Supplementary Information (ESI)

for

**Strong visible-light-absorbing BODIPY-based Cu(I) cyclic trinuclear sensitizers
for photocatalysis**

Ri-Qin Xia,^{a†} Ji Zheng,^{a†} Rong-Jia Wei,^a Jiaying He,^b Dong-Qin Ye,^a Ming-De Li,^{*b}
Guo-Hong Ning^{a*} and Dan Li^{a*}

^aCollege of Chemistry and Materials Science, Guangdong Provincial Key Laboratory of Functional Supramolecular Coordination Materials and Applications, Jinan University, Guangzhou 510632, People's Republic of China.

^bDepartment of Chemistry and Key Laboratory for Preparation and Application of Ordered Structural Materials of Guangdong Province, Shantou University, Shantou, 515063, China.

E-mail: mdli@stu.edu.cn; guohongning@jnu.edu.cn, danli@jnu.edu.cn.

Contents

Section S1. Materials and Methods	2
1.1. Materials	2
1.2. Characterization	2
Section S2. Synthesis	4
2.1. Synthesis of HL, 1, 2	4
2.2. PMMA film fabrication of HL, 1, 2	6
Section S3. Supplementary Figures	7
3.1. NMR spectroscopy	7
3.2. Cyclic Voltammetry (CV)	11
3.3. X-ray Photoelectron Spectroscopy (XPS)	11
3.4. Single-crystal structure	12
3.5. Thermogravimetric Analysis (TGA)	15
3.6. Fourier Transform Infrared (FT-IR) Spectra	15
3.7. Power X-ray Diffraction (PXRD)	16
3.8. Solution-state UV-Vis Absorption Spectra	17
3.9. Solution-state Photoluminescence Spectra	19
3.10. Room-Temperature Photoluminescence Lifetime	20
3.11. Film-state Photoluminescence Spectra	21
3.12. Transient Absorption Spectra (TAs)	23
3.13. Computational Details	25
3.14. Photocatalytic reaction	33
3.15. Photooxidation stability test	50
References	52

Section S1. Materials and Methods

1.1. Materials

Starting materials, reagents, and solvents were purchased from commercial sources and used without further purification.

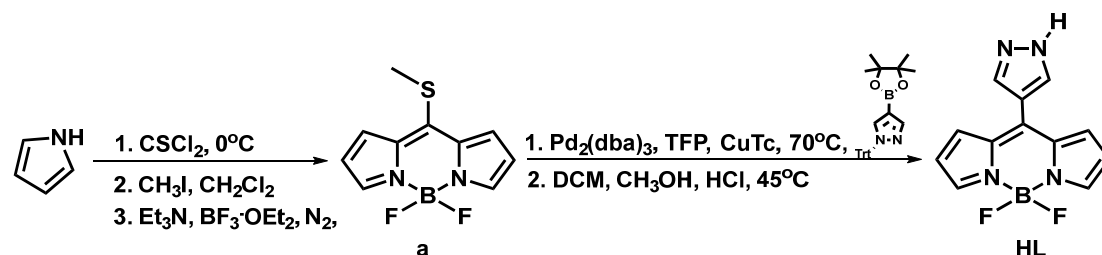
1.2. Characterization

Powder X-ray diffraction (PXRD) data was collected at 40 kV, 30 mA using microcrystalline samples on a Rigaku Ultima IV diffractometer using Cu-K α radiation ($\lambda = 1.5418 \text{ \AA}$). The measurement parameters include a scan speed of $0.5^\circ/\text{min}$, a step size of 0.02° , and a scan range of 2θ from 3° to 40° . Thermogravimetric analysis was performed on a Mettler-Toledo (TGA/DSC1) thermal analyzer. Measurement was made on approximately 5 mg of dried samples under a N₂ flow with a heating rate of $10^\circ\text{C}/\text{min}$. Fourier transform infrared (FT-IR) spectrum was measured using a Nicolet Avatar 360 FT-IR spectrophotometer. X-ray photoelectron (XPS) spectroscopy spectra were performed by a Thermo ESCALAB 250XI system. GC-MS analysis was carried out on an Agilent 7890B GC analyzer. Liquid ¹H and ¹³C NMR spectra were recorded on a Bruker Biospin Avance (400 MHz) equipment using tetramethylsilane (TMS) as an internal standard. Photooxidation reactions of DHN and thioanisole were performed with a 10 W LED flow reactor WP-TEC-1020HSL (WATTCAS, China), and photooxidation reaction of 4-formylphenylboronic acid was performed with a 300 W Xeon lamp. Femtosecond to Nanosecond Transient Absorption Spectroscopy (fs-TA and ns-TA) Experiments. The fs-TA measurements were performed based on a femtosecond Ti:sapphire regenerative amplifier laser system (Coherent, Astrella-Tunable-F-1k) and an fs-TA spectrometer system (Ultrafast Systems, Helios Fire). The detailed description of fs-TA was reported previously^{1,2}. In brief, fs-TA spectra were obtained by employing the harmonic 380 nm for the pump pulse and white-light continuum (330–800 nm light) for the probe pulse generated from the 800 nm output of a femtosecond regenerative amplified Ti:sapphire laser system. For the measurements, herein, the sample solution was excited in a 2 mm path-length cuvette. The subnanosecond transient absorption (EOS) experiment utilizes a subnanosecond

pulsed probe light source, a photonic crystal fiber (PCF)-based supercontinuum laser. The pulse duration of this probe determines the time resolution of the spectrometer (<1 ns). In EOS, the pump-probe delay is controlled electronically, and the maximum time window is close to half the repetition period of the pump laser. In our case, the maximum time window is $400 \mu\text{s}$. The sample solutions of CP employed in the ns-TA experiments were the same as in the fs-TA. Electron Paramagnetic Resonance (EPR) analysis was carried out on Bruker Magnettech ESR5000 in ESI, Bruker A300 in article.

Section S2. Synthesis

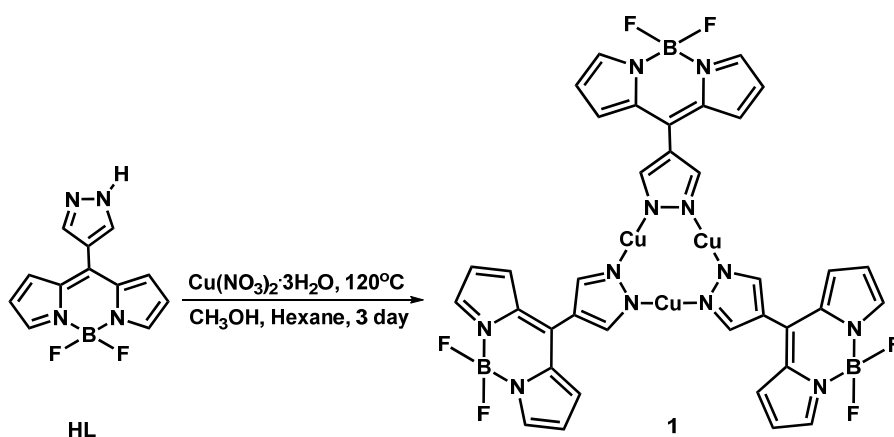
2.1. Synthesis of HL, 1, 2



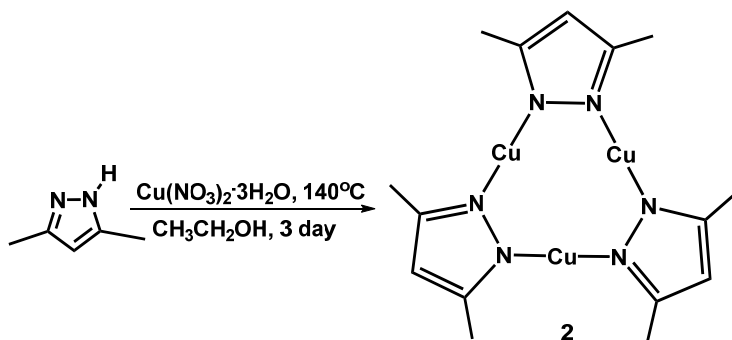
5,5-difluoro-10-(methylthio)-5H-4(1,5)-dipyrrolo[1,2-c:2',1'-f][1,3,2]diazaborinine (a). Compound **a** was synthesized according to the reported literatures.^{3,4} The ^1H , ^{13}C NMR spectra of **a** were shown in Figs. S1-S2. ^1H NMR (400 MHz, 298K, CDCl_3) δ 7.80 (s, 2H, CH), 7.42 (d, $J = 4.2$ Hz, 2H, CH), 6.53 (d, $J = 3.9$ Hz, 2H, CH), 2.91 (s, 3H, CH_3) ppm. ^{13}C NMR (100 MHz, 298K, CDCl_3) δ 153.93, 141.33, 127.62, 20.37 ppm.

5,5-difluoro-10-(1H-pyrazol-4-yl)-5H-4(1,5)-dipyrrolo[1,2-c:2',1'-f][1,3,2]diazaborinine (HL). **a** (1.05 g, 4.5 mmol), 4-(4,4,5,5-tetramethyl-1,3,2-dioxaborolan-2-yl)-1-trityl-1H-pyrazole (5.89 g, 13.5 mmol), $\text{Pd}_2(\text{dba})_3$ (1.24 g, 30% mmol), trifurylphosphine (104.48 mg, 10% mmol), Cu(I)-2-thienylcarboxylate (2.15 g, 11.25 mmol) were mixed with 150 mL of THF, and the mixture was added to a dried 350 mL Schlenk flask. The reaction system was heated to reflux and stirred for 72 h under N_2 atmosphere, the reaction mixture was cooled down to room temperature and filtered and the filtrate was concentrated, followed by the purification of the mixture by silica gel column chromatography (CH_2Cl_2 /hexane, 2:1, v/v) to give orange-red solid (1.6 g, 71%). The obtained orange-red solid was dissolved in a mixture of CH_2Cl_2 /MeOH (1:1, v/v, 35 mL), into which 5.2 mL of 2 M hydrochloric acid was added. The mixture was heated to 45°C and stirred for 6 hours. The reaction was monitored by TLC, the pH of the solution was adjusted to about 7 with sodium carbonate solution after the reaction. Followed by the purification of the mixture by silica gel column chromatography (ethyl acetate/hexane, 1:1, v/v) to give red solid (78 mg, 48%). The ^1H , ^{19}F , ^{13}C NMR spectra of **HL** were shown in Figs. S3-S5. ^1H NMR (400 MHz, 298 K, $\text{DMSO}-d_6$) δ 13.81 (s, 1H, NH), 8.58

(s, 1H, CH), 8.12 (s, 1H, CH), 8.03 (s, 2H, CH), 7.42 (d, $J = 4.5$ Hz, 2H, CH), 6.68 (d, $J = 4.9$ Hz, 2H, CH) ppm. ^{19}F NMR (376 MHz, 298 K, DMSO- d_6) δ -141.92 – -141.68 (m) ppm. ^{13}C NMR (100 MHz, 298 K, DMSO- d_6) δ 143.21, 141.40, 140.08, 133.47, 131.00, 118.88, 114.61 ppm. IR (KBr, cm^{-1}) 3362 (s, N-H), 3128 (w, N-H), 2960 (w, C-H), 1543 (s, C=N), 1476 (m), 1392 (s), 1262 (m), 1124 (s), 1084 (s), 847 (m), 771 (m), 628 (w), 576 (w). Elemental analysis (CHN), $\text{C}_{12}\text{H}_9\text{BF}_2\text{N}_4$, calculated (%): C 55.86, H 3.52, N 14.73; found (%): C 55.32, H 3.76, N 21.56.



1. Ligand **HL** (39 mg, 0.15 mmol) and $\text{Cu}(\text{NO}_3)_2 \cdot 3\text{H}_2\text{O}$ (39 mg, 0.16 mmol) were dissolved in a solution of MeOH/hexane (2:1, v/v, 3 mL), into which 20 μL pyridine was added. The mixture was sealed in a Pyrex tube and kept in an oven at 120 $^\circ\text{C}$ for 72 h. Slowly cooling to room temperature gave complex **1** as dark red block crystals. Yield: 35%. The ^1H , ^{19}F , ^{13}C NMR spectra of **1** were shown in Figs. S4-S6. ^1H NMR (400 MHz, 298 K, DMSO- d_6) δ 8.36 (d, $J = 9.7$ Hz, 1H, CH), 8.00 (s, 1H, CH), 7.42 (s, 1H, CH), 6.69 (s, 1H, CH) ppm. ^{19}F NMR (376 MHz, 298 K, DMSO- d_6) δ -141.65 – -141.86 (m) ppm. ^{13}C NMR (100 MHz, 298 K, DMSO- d_6) δ 143.58, 142.36, 140.35, 133.27, 130.06, 118.61, 114.31 ppm. IR (KBr, cm^{-1}) 3445(w, N-H), 3120 (w, N-H), 2968 (w, C-H), 1545 (s, C=N), 1468 (m), 1393 (s), 1266 (m), 1124 (m), 1081 (s), 851 (m), 772 (m), 664 (m), 578 (w). Elemental analysis (CHN), $\text{C}_{36}\text{H}_{24}\text{B}_3\text{Cu}_3\text{F}_6\text{N}_{12}(\text{H}_2\text{O})_3$, calculated (%): C 42.57, H 2.98, N 16.55; found (%): C 42.83, H 2.46, N 16.08.



2. Complex **2** was prepared according to reported literature procedures with slight modification.^{5, 6} Ligand 3,5-dimethylpyrazole (96 mg, 1.0 mmol) and $\text{Cu}(\text{NO}_3)_2 \cdot 3\text{H}_2\text{O}$ (120.8 mg, 0.5 mmol) were dissolved in a mixture of EtOH/Chlorobenzene (2:1 v/v, 3 mL). The mixture was sealed in a Pyrex tube and kept in an oven at 140 °C for 72 h. Slowly cooling to room temperature gave complex **2** as yellowish block crystals. Yield: 65%. IR (KBr, cm^{-1}) 2961 (w, C-H), 1524 (s, C=N), 1421 (m), 1345 (m), 1148 (m), 1058 (m), 768 (s), 651 (w), 593 (w). Elemental analysis (CHN), $\text{C}_{15}\text{H}_{21}\text{Cu}_3\text{N}_6$, calculated (%): C 37.85, H 4.45, N 17.66; found (%): C 37.40, H 4.35, N 17.52.

2.2. PMMA film fabrication of **HL**, **1**, **2**

Sample (0.002 mmol) and 100 mg polymethyl methacrylate (PMMA) are dissolved in a mixed solution of dimethyl sulfoxide (DMSO) and CH_2Cl_2 (1:4, v/v, 5 mL), and then they are applied to a glass plate and air-dried to form a film.

Section S3. Supplementary Figures

3.1. NMR spectroscopy

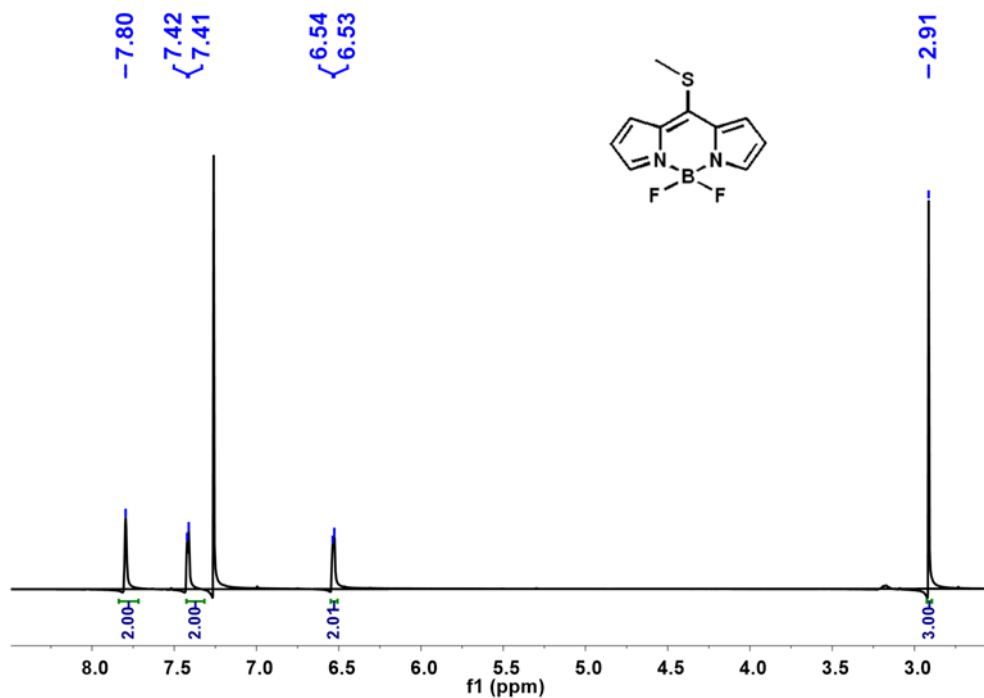


Fig. S1. ^1H NMR spectrum (400 MHz, 298 K, DMSO-d_6) of **a**.

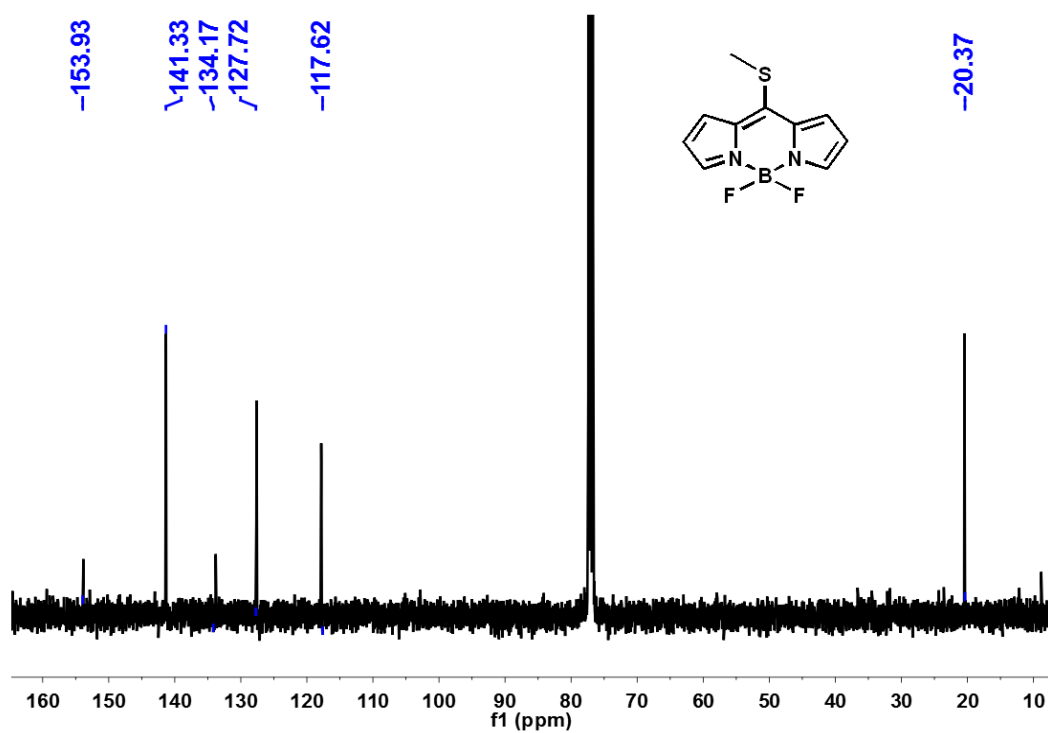


Fig. S2. ^{13}C NMR spectrum (100 MHz, 298 K, DMSO-d_6) of **a**.

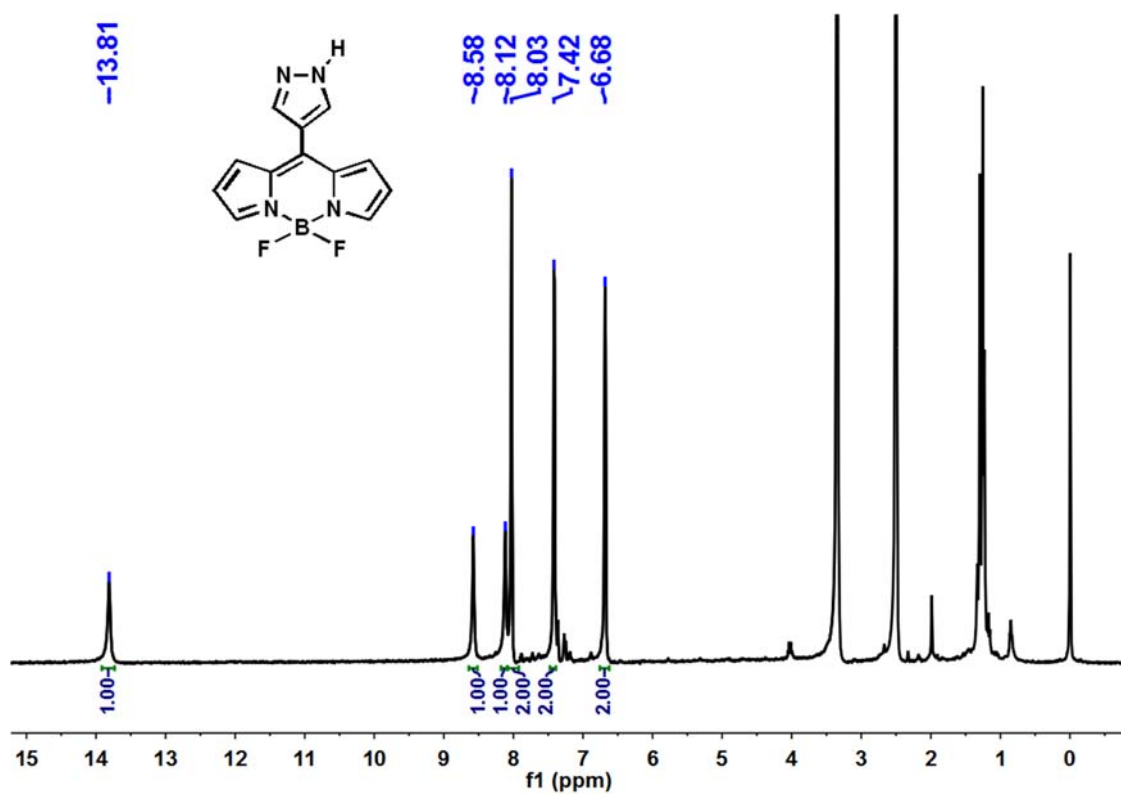


Fig. S3. ¹H NMR spectrum (400 MHz, 298 K, DMSO-d₆) of HL.

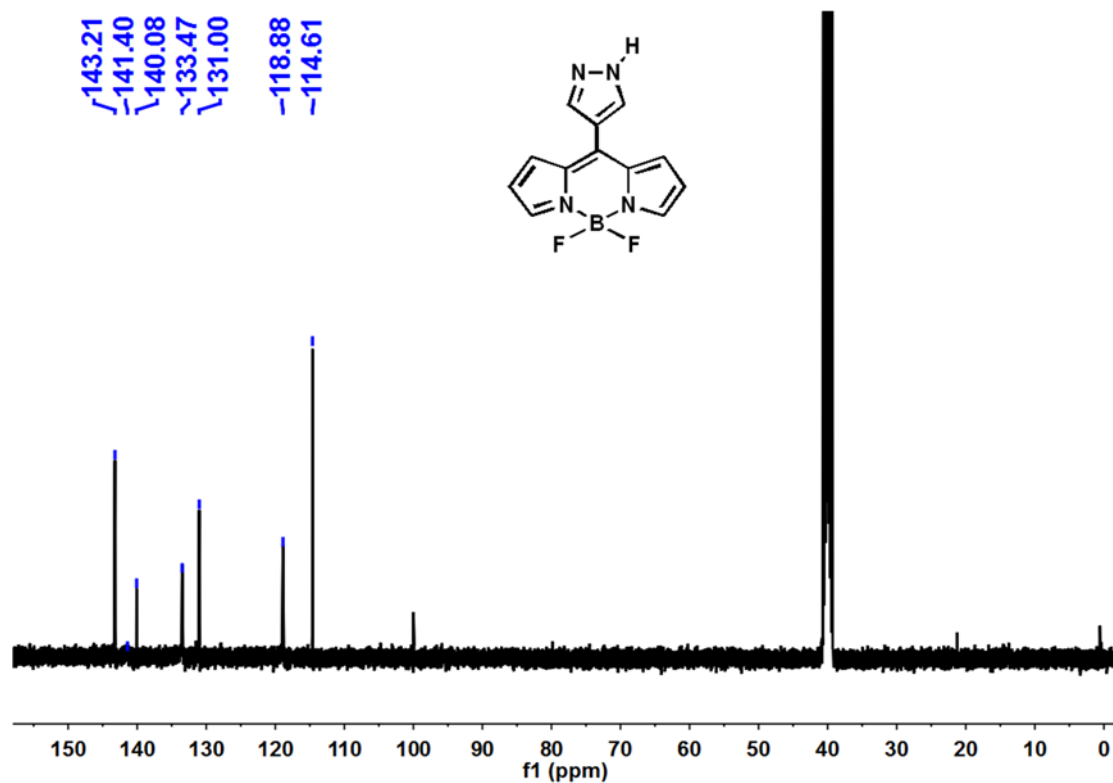


Fig. S4. ¹³C NMR spectrum (100 MHz, 298 K, DMSO-d₆) of HL.

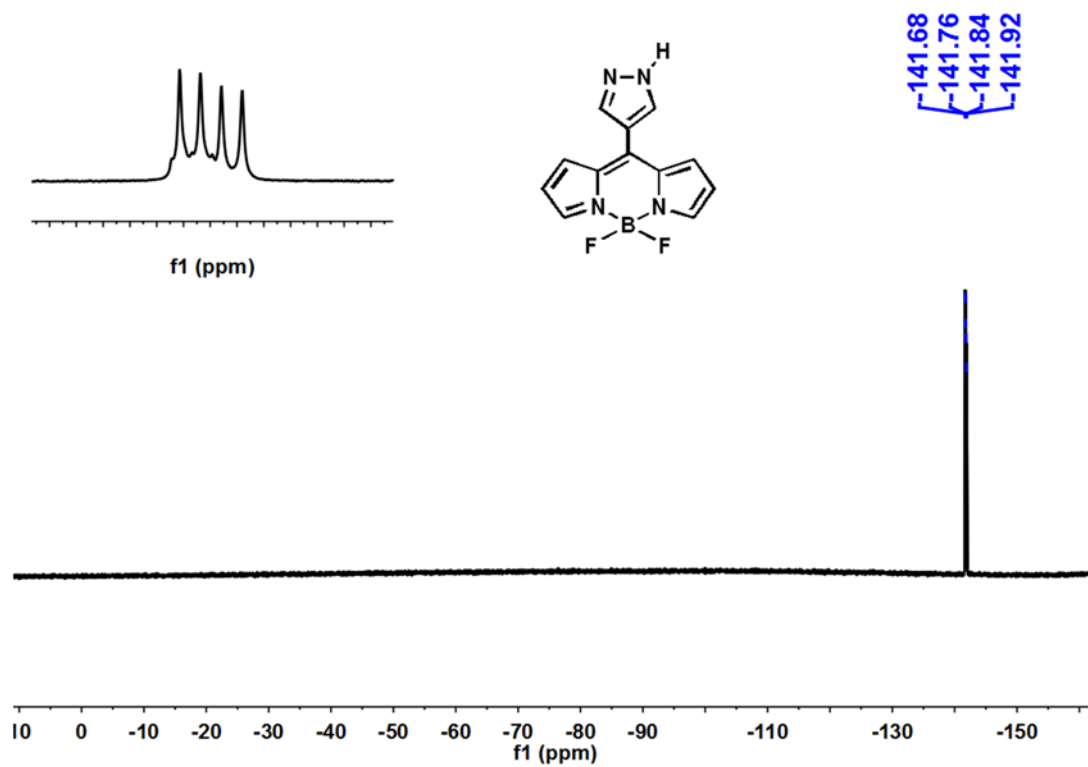


Fig. S5. ^{19}F NMR spectrum (376 MHz, 298 K, DMSO-d_6) of **HL**.

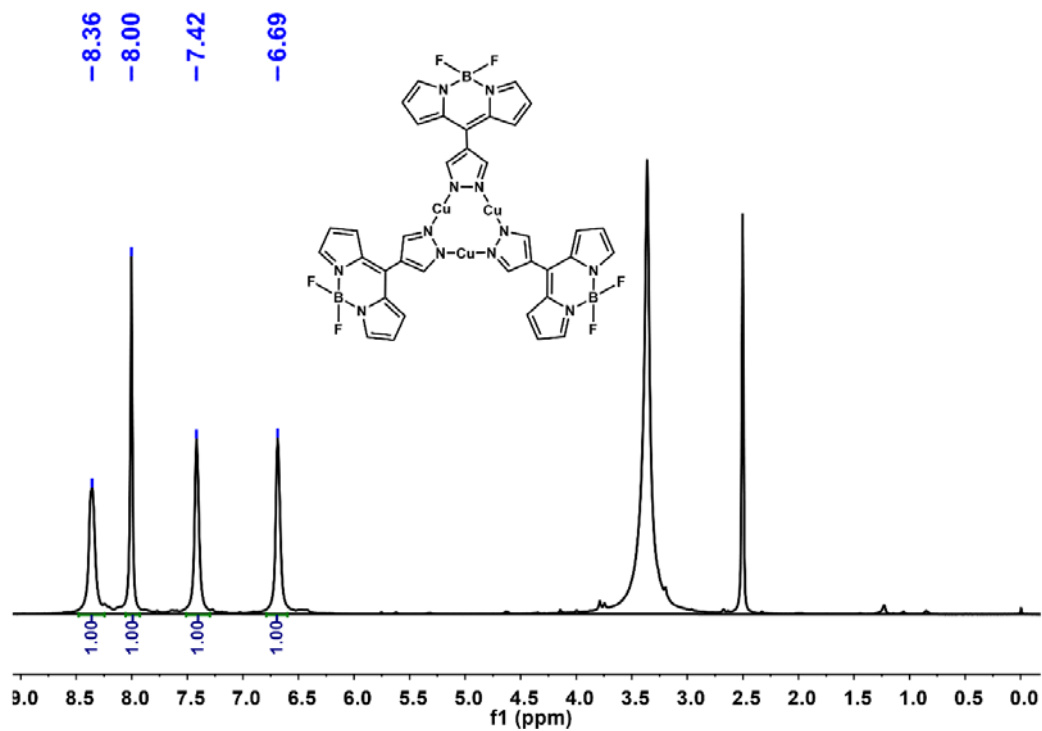


Fig. S6. ^1H NMR spectrum (400 MHz, 298 K, DMSO-d_6) of **1**.

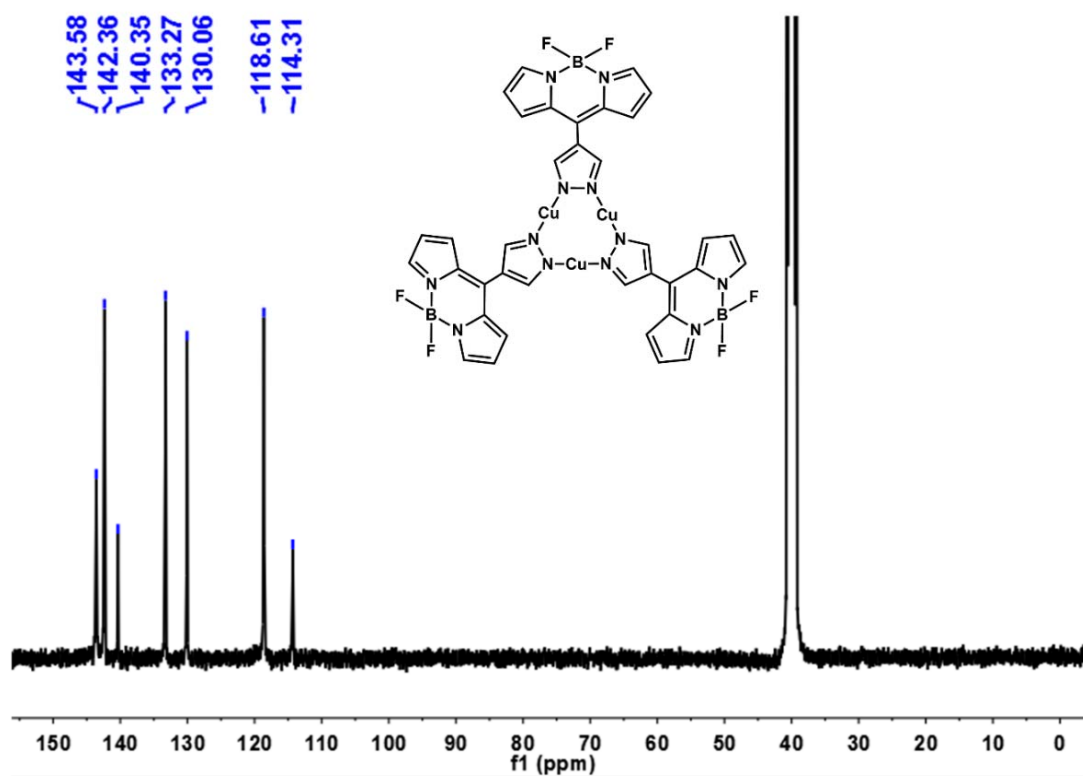


Fig. S7. ^{13}C NMR spectrum (100 MHz, 298 K, DMSO- d_6) of **1**.

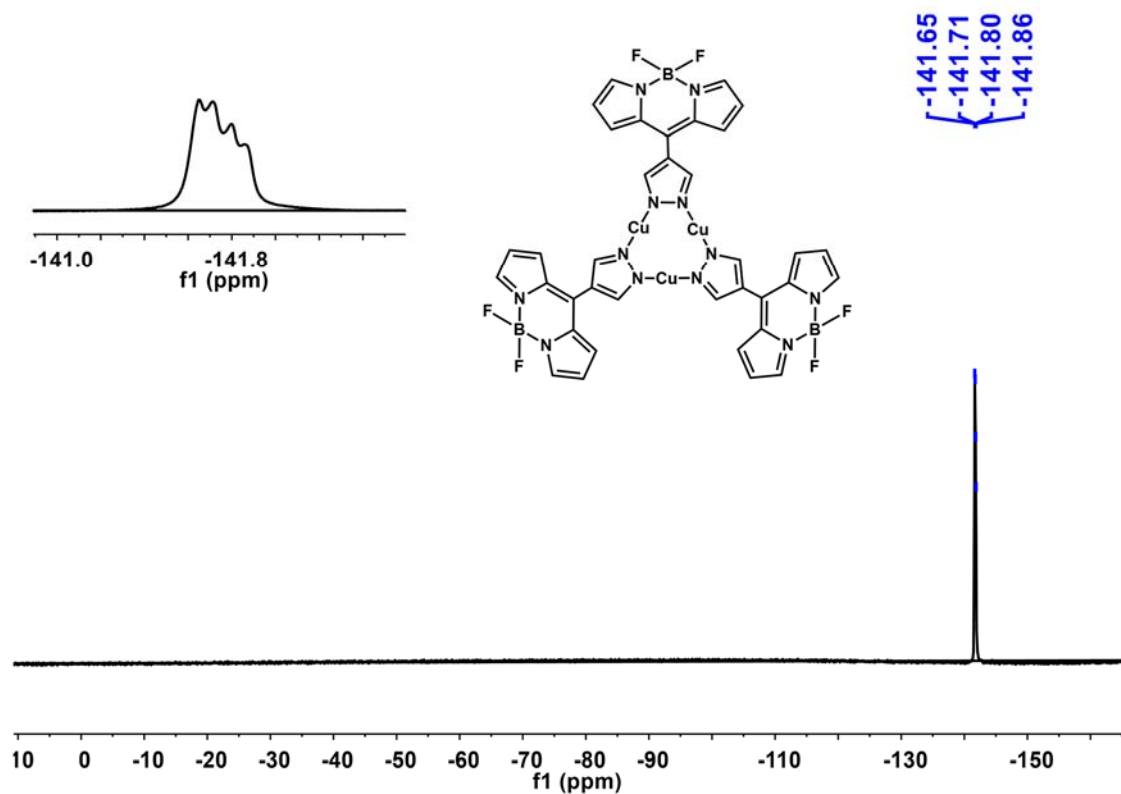


Fig. S8. ^{19}F NMR spectrum (376 MHz, 298 K, DMSO- d_6) of **1**.

3.2. Cyclic Voltammetry (CV)

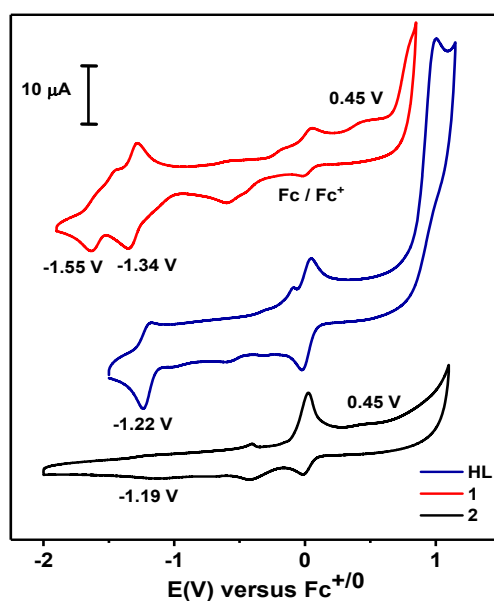


Fig. S9. CV curves of **HL**, **1**, and **2**. The experiments were carried out in deaerated DMF solution, containing 0.5 mM of **HL**, **1**, or **2**, 0.2 mM ferrocene, and 0.10 M Bu₄NPF₆ as the supporting electrolyte, with a scan rate of 0.05 V/s⁻¹ and a negative initial scan direction. Glassy carbon electrode, Ag/AgNO₃, and Pt silk were used as the working electrode, reference electrode, and counter electrode, respectively.

3.3. X-ray Photoelectron Spectroscopy (XPS)

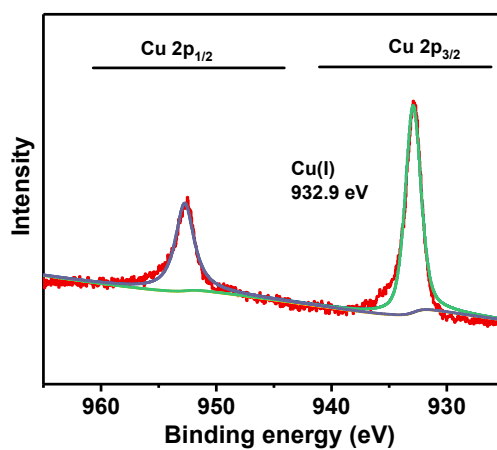


Fig. S10. XPS of **1**.

3.4. Single-crystal structure

Suitable single crystals of **1** and **2** were mounted with nylon loops. Data was collected on an Oxford Diffraction XtalAB [Rigaku(Cu) Xray dual wavelength source, $K\alpha$, $\lambda = 1.5418 \text{ \AA}$] equipped with a monochromator and CCD plate detector (CrysAlisPro CCD, Oxford Diffraction Ltd) at 100 K. Single-crystal structures of compounds **1** and **2** were solved by direct methods by ShelXS⁷ in Olex2 1.3⁸. All non-hydrogen atoms were refined with anisotropic thermal parameters, and all hydrogen atoms were included in calculated positions and refined with isotropic thermal parameters riding on those of the parent atoms. Crystal data and structure refinement parameters were summarized in Table S1.

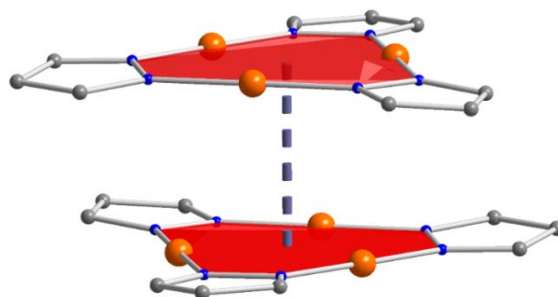


Fig. S11. The dimer of **1** in the crystal and the dash line refers to the distance between the Cu_3N_6 planes (3.214 \AA). Hydrogen atoms and BODIPY units were omitted for clarity. Color code: Cu, orange; N, blue; C, gray.

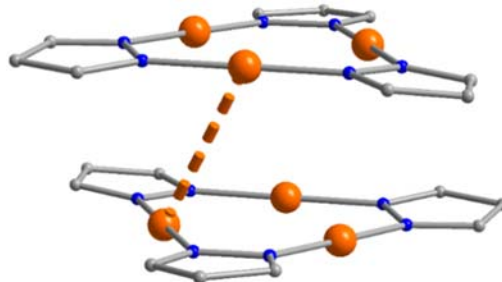


Fig. S12. Stacked diagram of two molecules for **1**, and the distance between $\text{Cu}\cdots\text{Cu}$ is 3.734 \AA . Hydrogen atoms and BODIPY units were omitted for clarity. Color code: Cu, orange; N, blue; C, gray.

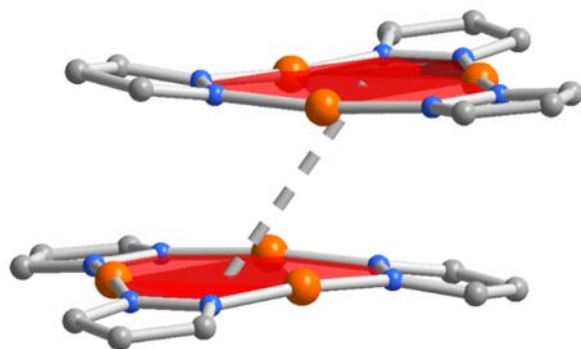


Fig. S13. The dimer of **2** in the crystal and the dash line refers to the distance between the Cu_3N_6 planes (3.745 \AA). Hydrogen atoms and methyl substituents were omitted for clarity. Color code: Cu, orange; N, blue; C, gray.

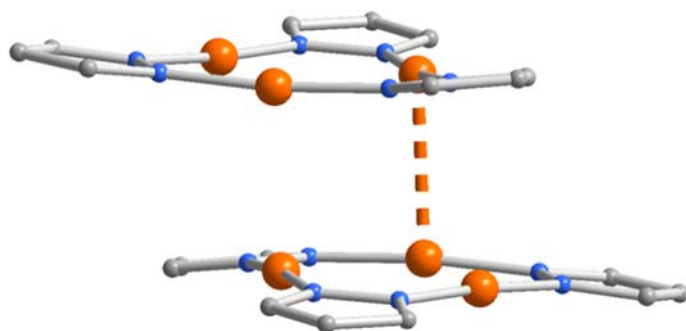


Fig. S14. Stacked diagram of two molecules for **2**, and the distance between $\text{Cu}\cdots\text{Cu}$ is 2.887 \AA . Hydrogen atoms and methyl substituents were omitted for clarity. Color code: Cu, orange; N, blue; C, gray.

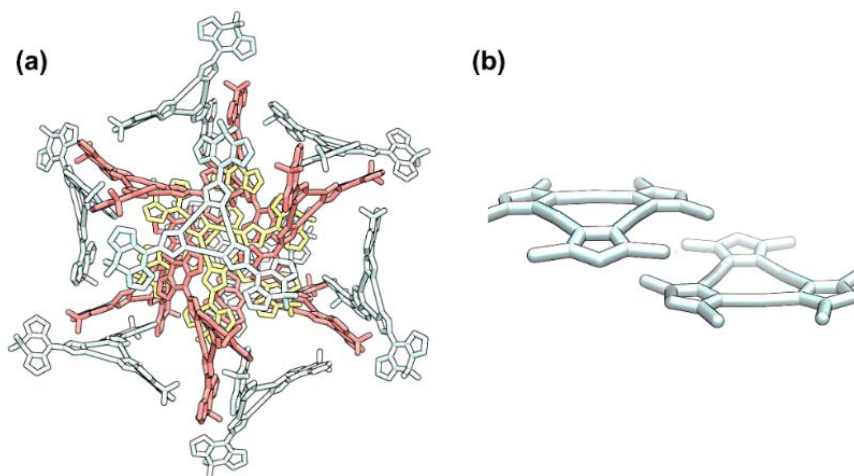


Fig. S15. Crystal packing in one unit cell. (a) **1**; (b) **2**.

Table S1. Crystal data and structure refinement parameters of **1** and **2**.

Parameter	1	2
Empirical formula	C ₃₆ H ₂₄ B ₃ Cu ₃ F ₆ N ₁₂	C ₁₅ H ₂₁ Cu ₃ N ₆
Formula weight	961.72	476.00
Temperature/K	99.97	100.00
Crystal system	cubic	triclinic
Space group	<i>Ia-3</i>	<i>P-1</i>
a/Å	24.8754(2)	8.4090(3)
b/Å	24.8754(2)	10.1687(4)
c/Å	24.8754(2)	11.3477(4)
α /°	90.000	70.031(3)
β /°	90.000	75.972(3)
γ /°	90.000	82.051(3)
Volume/Å ³	15392.5(4)	883.15(6)
Z	16	2
$\rho_{\text{calc}}/\text{cm}^3$	1.660	1.790
μ/mm^{-1}	2.583	4.260
F(000)	7680	480
2 θ range for data collection/°	4.3310 to 74.3740	4.239 to 78.358
Index ranges	-30 ≤ h ≤ 15 -20 ≤ k ≤ 28 -23 ≤ l ≤ 27	-10 ≤ h ≤ 10 -12 ≤ k ≤ 12 -14 ≤ l ≤ 14
Reflections collected	9120	7777
Independent reflections	2643 [<i>R</i> _{int} = 0.0217, <i>R</i> _{sigma} = 0.060]	3599 [<i>R</i> _{int} = 0.0433, <i>R</i> _{sigma} = 0.172]
Data/restraints/parameters	2643 / 0 / 181	3599 / 0 / 223
Largest diff. peak and hole (e/Å ³)	0.369, -0.333	0.989, -1.122
Goodness-of-fit on F ²	1.076	1.116
<i>R</i> ₁ ^a [<i>I</i> ≥ 2σ(<i>I</i>)]	0.0431	0.0586
<i>wR</i> ₂ ^b (all data)	0.1241	0.1727
CCDC Nos.	2072182	2133483

$$^a R_1 = \sum(|F_o| - |F_c|) / \sum F_o; \quad ^b wR_2 = [\sum w(F_o^2 - F_c^2)^2 / \sum w(F_o^2)^2]^{1/2}$$

3.5. Thermogravimetric Analysis (TGA)

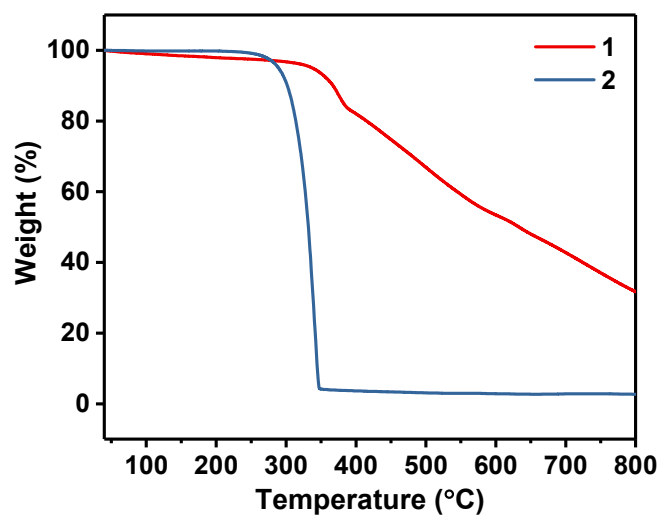


Fig. S16. TGA profiles of **1** and **2** under N₂ atmosphere.

3.6. Fourier Transform Infrared (FT-IR) Spectra

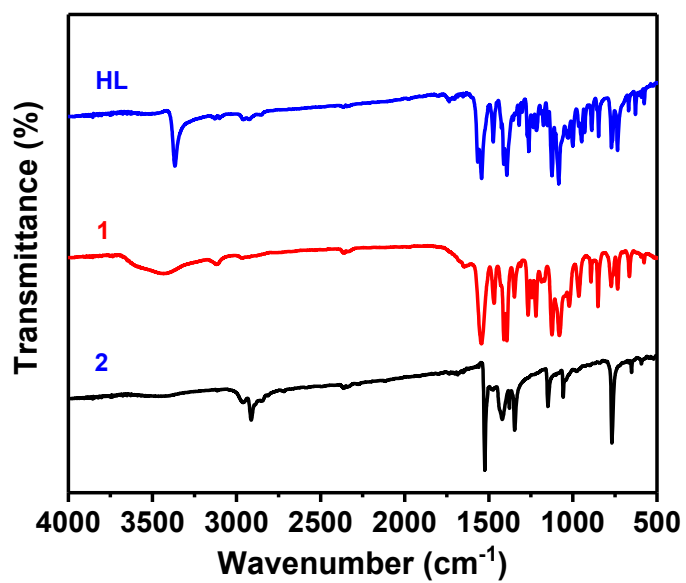


Fig. S17. FT-IR spectra of **HL**, **1**, and **2**.

3.7. Power X-ray Diffraction (PXRD)

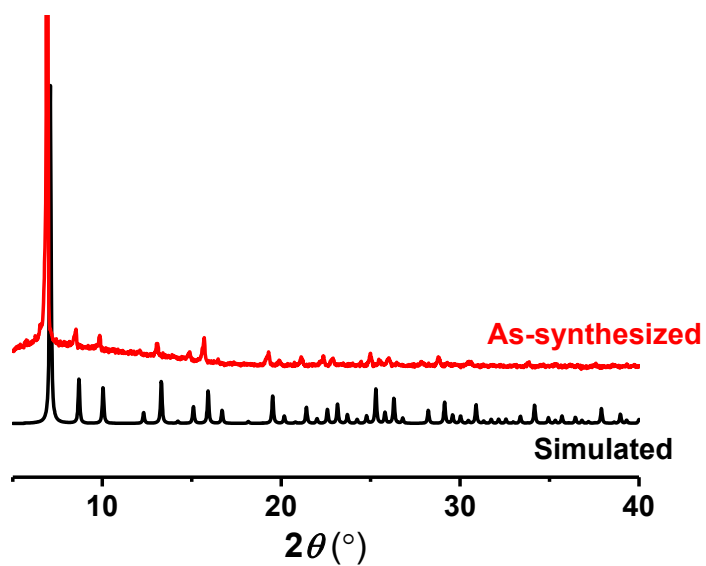


Fig. S18. The comparison of simulated and as-synthesized PXRD patterns of **1**.

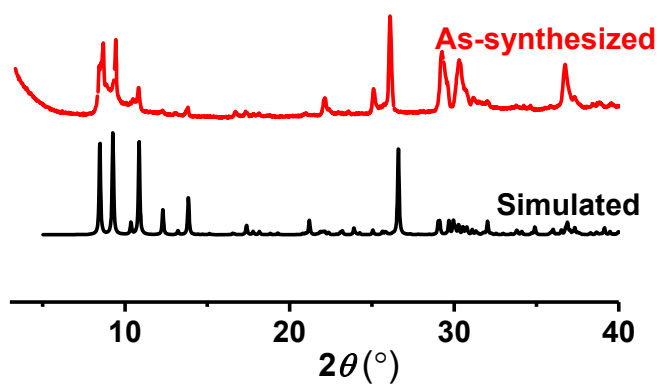


Fig. S19. The comparison of simulated and as-synthesized PXRD patterns of **2**.

3.8. Solution-state UV-Vis Absorption Spectra

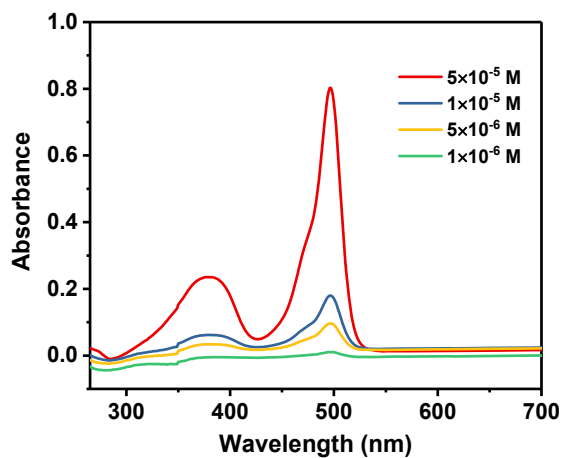


Fig. S20. UV-Vis absorption spectra of **HL** in DMSO.

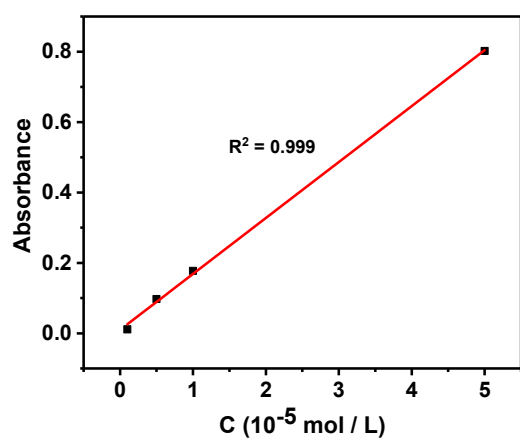


Fig. S21. Absorbance-concentration fitting curve of **HL**, $R^2 = 0.999$.

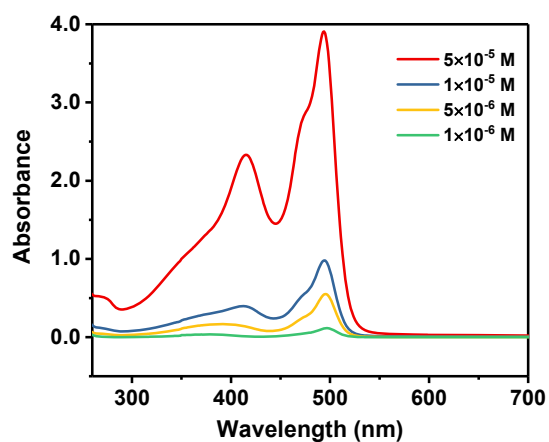


Fig. S22. UV-Vis absorption spectra of **1** in DMSO.

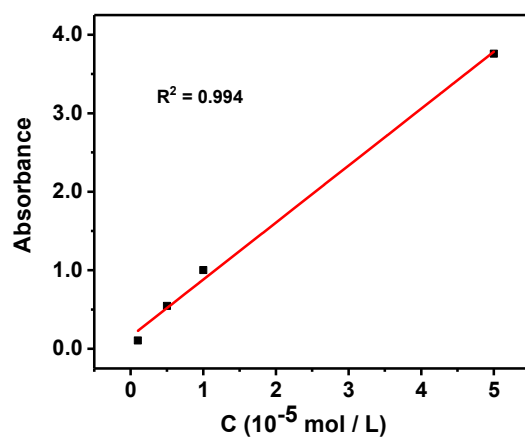


Fig. S23. Absorbance-concentration fitting curve of **1**. $R^2 = 0.994$.

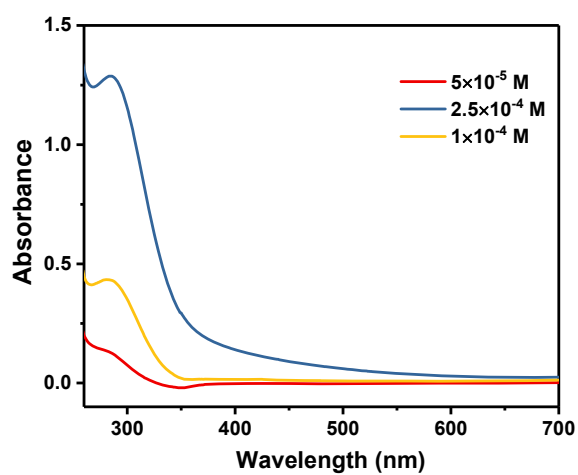


Fig. S24. UV-Vis absorption spectra of **2** in DMSO.

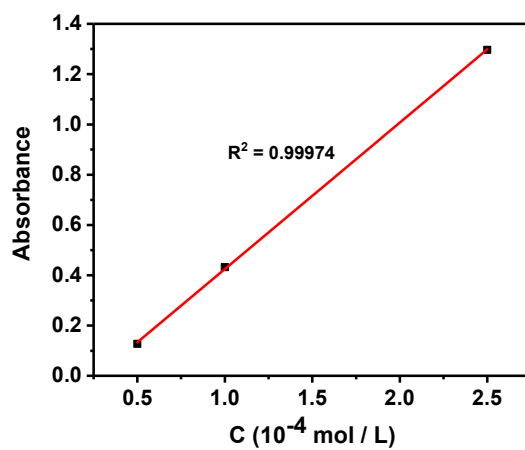


Fig. S25. Absorbance-concentration fitting curve of **2**. $R^2 = 0.999$.

3.9. Solution-state Photoluminescence Spectra

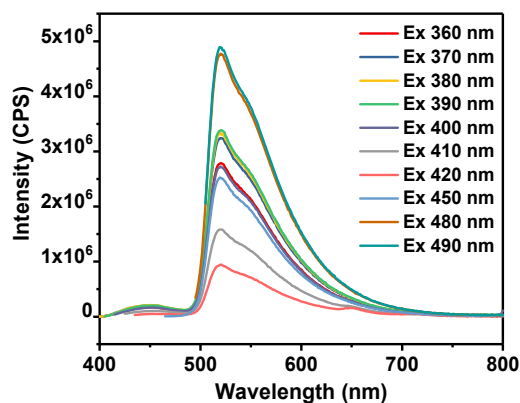


Fig. S26. The room-temperature emission spectra of **1** in DMSO (1×10^{-5} M) under different excitation wavelengths.

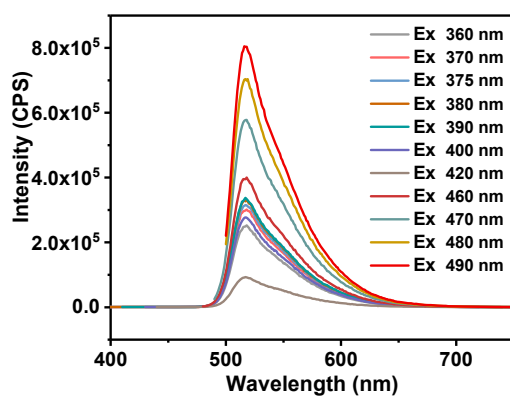


Fig. S27. The room-temperature emission spectra of **HL** in DMSO (1×10^{-5} M) under different excitation wavelengths.

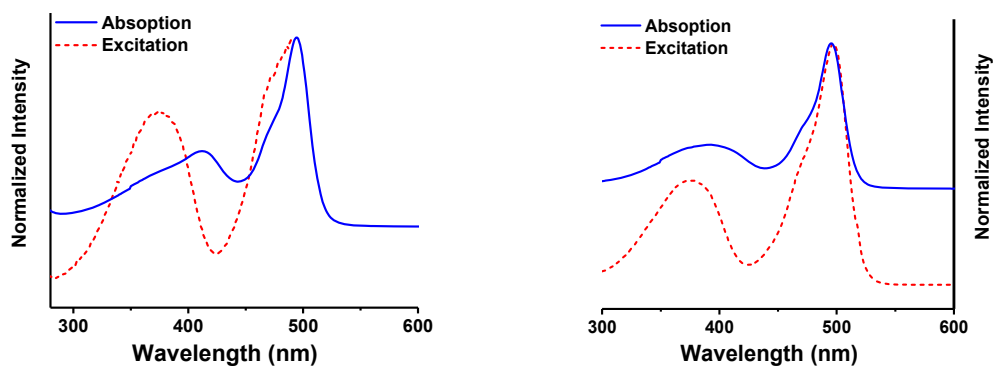


Fig. S28. Comparison of normalized UV-vis absorption and excitation spectra of complex **1** at different concentrations, 1×10^{-5} M (left); 5×10^{-6} M (right).

3.10. Room-Temperature Photoluminescence Lifetime

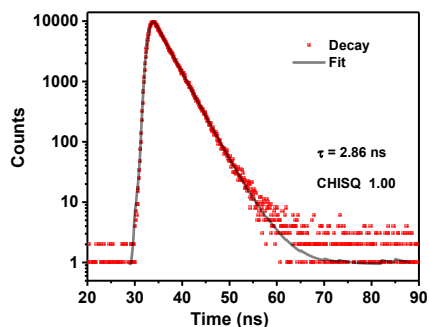


Fig. S29. Photoluminescence decay of **HL** ($C = 1 \times 10^{-5}$ M) obtained via time-correlated single photon counting (red), and the black line represents a dual-exponential fit of the data.

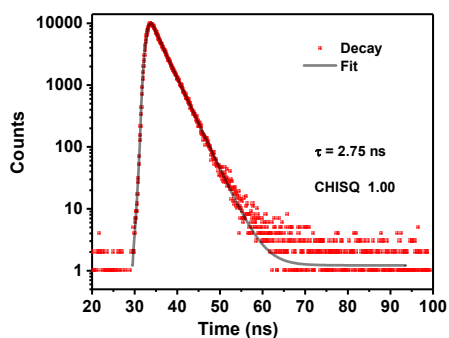


Fig. S30. Photoluminescence decay of **1** ($C = 1 \times 10^{-5}$ M) obtained via time-correlated single photon counting (red), and the black line represents a dual-exponential fit of the data.

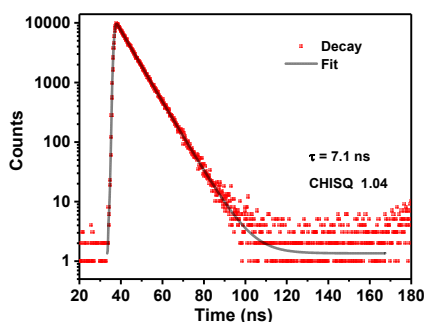


Fig. S31. Photoluminescence decay of **HL** at film-state obtained via time-correlated single photon counting (red), and the black line represents a dual-exponential fit of the data.

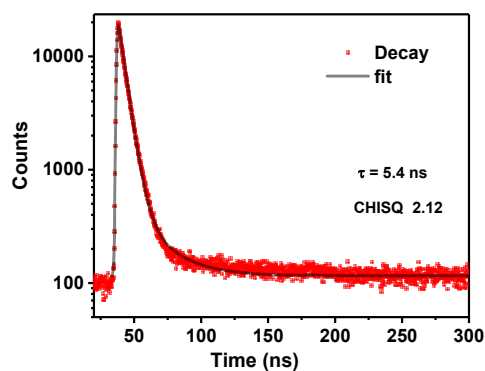


Fig. S32. Photoluminescence decay of **1** at film-state obtained via time-correlated single photon counting (red), and the black line represents a dual-exponential fit of the data.

3.11. Film-state Photoluminescence Spectra

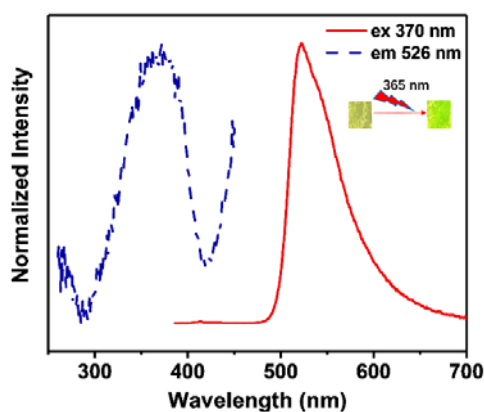


Fig. S33. Comparison of normalized emission and excitation spectrum of **HL**.

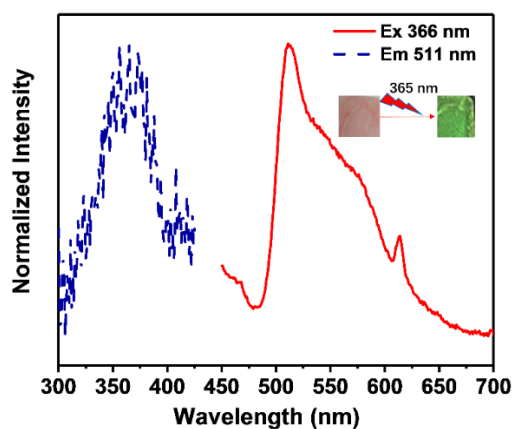


Fig. S34. Comparison of normalized emission and excitation spectrum of **1**.

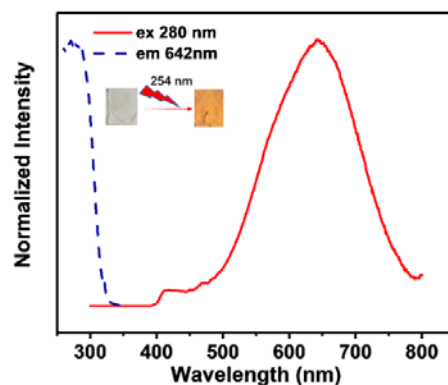


Fig. S35. Comparison of normalized emission and excitation spectrum of **2**.

Table S2. Summary of photophysical parameters for the compounds in the film state

complexes	λ_{ex}	λ_{em}	Φ_{F} (%) ^a	τ_{F} (ns) ^d	τ_{T} (μs) ^g
HL	370	526	91.9 ^b	7.1 ^e	0.6 ^h
1	366	511	2.9 ^b	5.4 ^e	1.0 ^h
2	280	642	100 ^c	1.9 ^f	19 ⁱ

^a Fluorescence quantum yields. ^b $\lambda_{\text{ex}} = 370$ nm. ^c $\lambda_{\text{ex}} = 280$ nm. ^d The average fluorescence decay lifetime. ^e $\lambda_{\text{ex}} = 370$ nm. ^f $\lambda_{\text{ex}} = 320$ nm. ^g The average phosphorescence decay lifetime. ^h $\lambda_{\text{ex}} = 370$ nm. ⁱ $\lambda_{\text{ex}} = 340$ nm.

3.12. Transient Absorption Spectra (TAs)

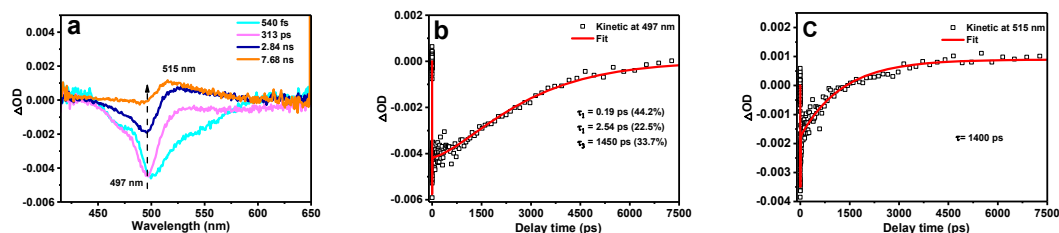


Fig. S36. Femtosecond transient absorption spectra of (a) **HL**; (b) The decay of **HL** at 497 nm; c) The decay of **HL** at 516 nm, $C = 1 \times 10^{-5}$ M in DMSO solution after pulsed excitation at 380 nm.

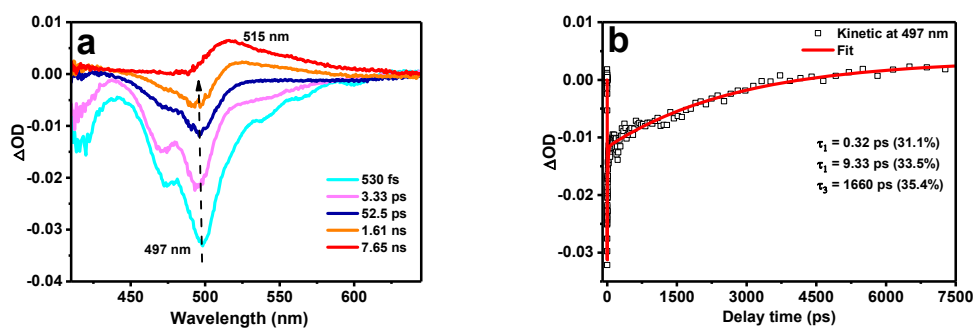


Fig. S37. Femtosecond transient absorption spectra of (a) **1**; (b) The decay of **1** at 497 nm, $C = 1 \times 10^{-5}$ M in DMSO solution after pulsed excitation at 380 nm.

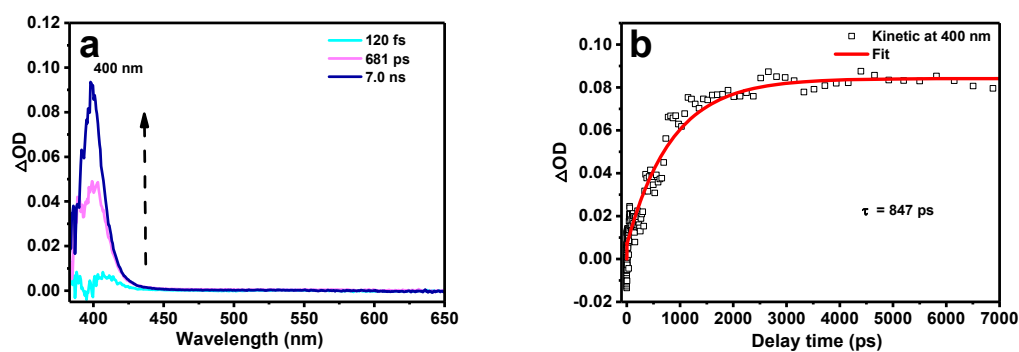


Fig. S38. Femtosecond transient absorption spectra of (a) **2**; (b) the decay of **2** at 400 nm, $C = 1 \times 10^{-5}$ M in DMSO solution after pulsed excitation at 380 nm.

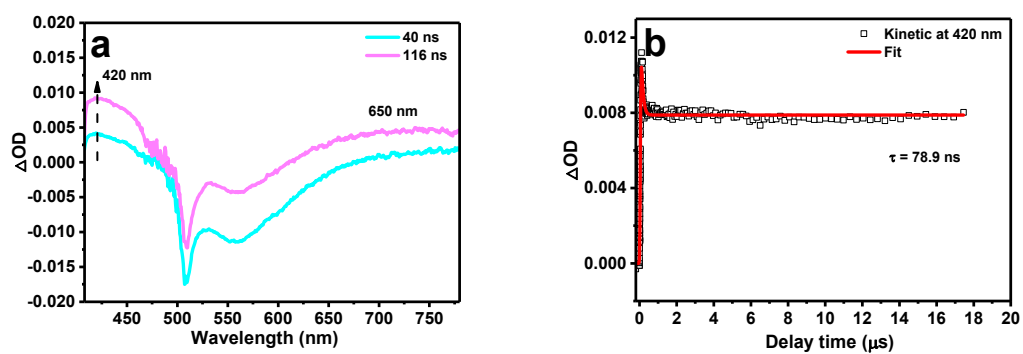


Fig. S39. Nanosecond transient absorption spectra of (a) **HL**; (b) the decay of **HL** at 420 nm, $C = 1 \times 10^{-5}$ M in deaerated DMSO solution after pulsed excitation at 400 nm.

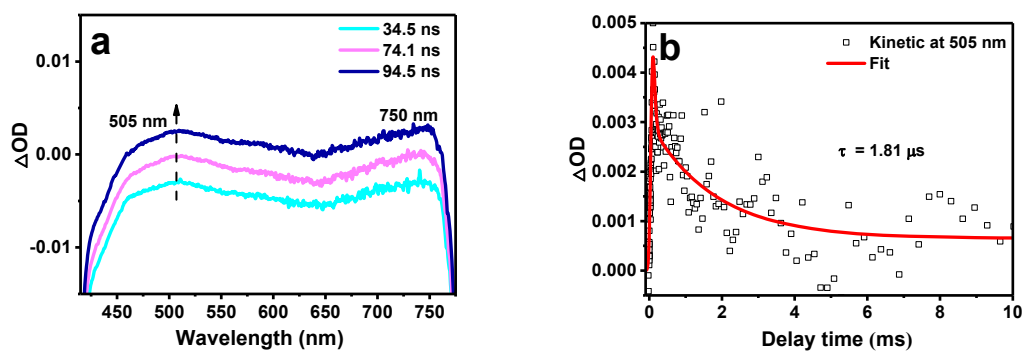


Fig. S40. Nanosecond transient absorption spectra of (a) **2**; (b) the decay of **2** at 505 nm, $C = 1 \times 10^{-5}$ M in deaerated DMSO solution after pulsed excitation at 400 nm.

3.13. Computational Details

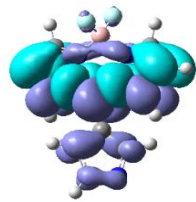
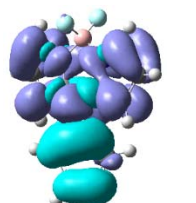
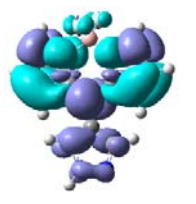
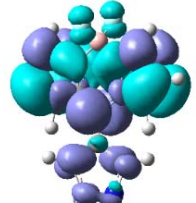
Density functional theory (DFT) as well as time-dependent density functional theory (TDDFT) computations were performed for ligand **HL** and complexes **1** and **2** by using Gaussian 09 software.⁹ The following level of theory was adopted in all the calculations: (1) Functional: the hybrid Perdew, Burke, and Ernzerhof functional (PBE0)^{10, 11} in conjunction with D3(BJ) dispersion correlation;^{12, 13} (2) Basis sets: the LANL2DZ¹⁴⁻¹⁷ effective core potential (ECP) was used for Cu and the 6-31G(d,p)¹⁸ basis set was used for the other atoms; (3) the solvent effect of DMSO was considered by using solvation model density (SMD).¹⁹ Firstly, the geometrical optimization was performed for the monomers of all the above compounds to obtain their stable ground-state (S_0) geometries by restricted PBE0 method, confirmed by the absence of imaginary frequencies (NIMG = 0). Then, the first 50 singlet-singlet spin-allowed transitions and the first 10 singlet-triplet spin-forbidden transitions were calculated based on the optimized S_0 structures. By using Multiwfn program,²⁰ the TDDFT results were extracted from the Gaussian output files (log files), and the cub files for drawing the electron density differences (EDD) maps were obtained by the hole-electron analysis function²¹ of Multiwfn software after inputting the logfiles and the formatted checkpoint (fchk) files. Note that before comparing the experimental and simulated UV-vis absorption spectra of **HL** and complexes **1** and **2**, the simulated wavelengths were multiplied by 1.2, since 1.2 is the result of experiment absorption maximum (497.0 nm) / simulated absorption maximum (410.8 nm) of **HL**. Besides, the cub files for drawing the contours of molecular orbitals of complex **1** and **2** were obtained by Multiwfn software after inputting the fchk files of TDDFT. The stable geometries of the first triplet state (T_1) for all the above three compounds were obtained by unrestricted PBE0 method. Spin density surfaces of T_1 states were drawn using the cub files generated by Multiwfn program. For complex **1**, the geometrical optimization and the calculations of the first singlet and triplet excited (S_1 and T_1) states were also carried out based on the dimer model extracted from the corresponding X-ray single-crystal data.

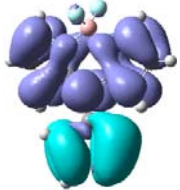
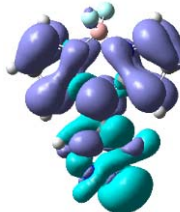
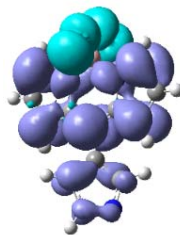
Table S3 The comparison of selected structural parameters between the geometries of S_0 and T_1 states of the monomers of ligand **HL** and complexes **1** and **2** optimized at PBE0-D3(BJ) level

	Torsion Angle ($^\circ$) ^a		$d_{\text{Cu-Cu}}$ (\AA) ^b	
	S_0	T_1	S_0	T_1
HL	39.2	42.3	-	-
1	37.8, 38.1, 38.3	37.6, 38.2, 42.6	3.216, 3.234, 3.234	3.221, 3.228, 3.228
2	-	-	3.204, 3.240, 3.240	2.707, 2.861, 2.862

^a The torsion angles between a BODIPY ring and a pyrazolyl ring. ^b The intermolecular Cu-Cu distances.

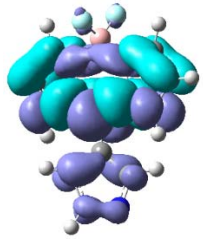
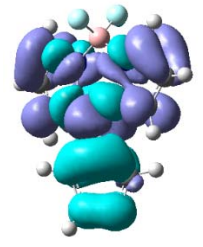
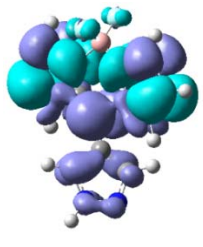
Table S4. The selected singlet-singlet spin-allowed transitions of **HL** in DMSO at PBE0-D3(BJ)/6-31G(d,p) level^a

No.	E(eV)	$\lambda(\text{nm})^b$	f^c	EDD map ^d
1	3.018	410.8 (493.0)	0.4905	
2	3.568	347.5 (417.0)	0.2574	
3	3.681	336.8 (404.2)	0.1076	
4	3.912	316.9 (380.3)	0.0815	

5	4.134	299.9 (359.9)	0.0197	
6	4.971	249.4 (299.3)	0.0300	
10	6.429	192.9 (231.4)	0.0131	

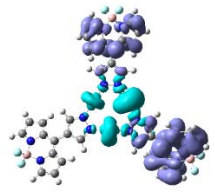
^a Only the TDDFT results of S₁ state and the S_n states with f larger than 0.01 among the first 10 S_n states were given. ^b The wavelengths multiplied by 1.2 were given in parentheses. ^c Oscillator strength. ^d Isovalue = 5×10⁻⁴ a.u. The electrons transfer from the blue regions to the purple regions during the excitation from S₀ state to S_n state.

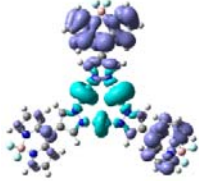
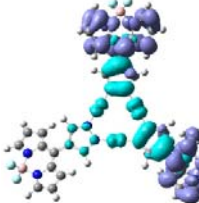
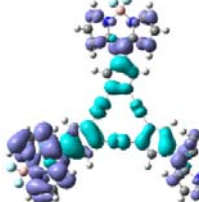
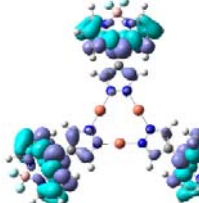
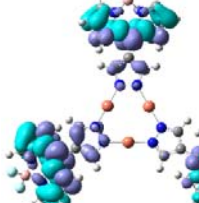
Table S5. The selected singlet-triplet spin-forbidden transitions of **HL** in DMSO at PBE0-D3(BJ)/6-31G(d,p) level^a

No.	E(eV)	λ (nm)	EDD map ^b
1	1.680	738.0	
2	2.738	452.8	
3	2.832	437.8	

^a Only the TDDFT results of the T_n states lower than S_1 state in energy were given. ^b Isovalue = 5×10^{-4} a.u. The electrons transfer from the blue regions to the purple regions during the excitation from S_0 state to T_n state.

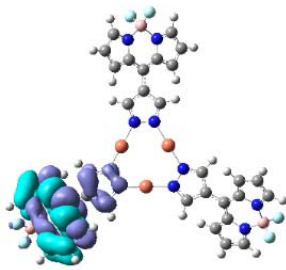
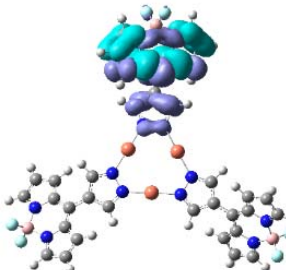
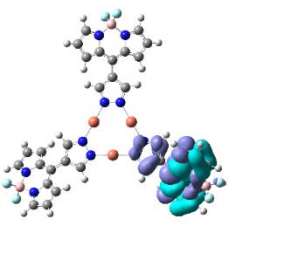
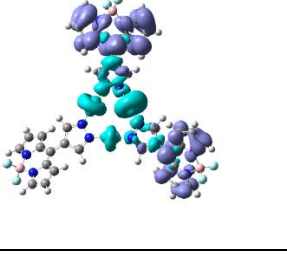
Table S6. The selected singlet-singlet spin-allowed transitions of complex **1** in DMSO at PBE0-D3(BJ)/(Lan12dz+6-31G(d,p)) level^a

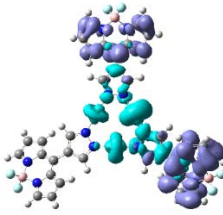
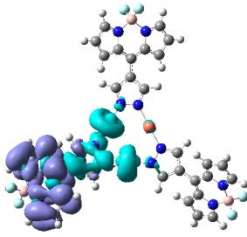
No.	E(eV)	λ (nm) ^b	f^c	EDD map ^d	Main transition ^e
1	2.505	495.0 (594.0)	0.0154		H \rightarrow L (58.5%), H \rightarrow L+2 (19.2%), H-1 \rightarrow L+2 (8.5%), H-1 \rightarrow L+1 (6.7%),

					H→L+1 (6.5%)
2	2.513	493.5 (592.2)	0.0101		H→L+2 (33.1%), H→L+1 (32.4%), H-1→L (31.0%)
7	2.993	414.3 (497.1)	0.4826		H-5→L (57.0%), H-5→L+1 (11.7%), H-6→L+2 (10.2%), H-5→L+2 (8.2%), H-6→L+1 (6.9%)
8	2.998	413.6 (496.3)	0.4918		H-6→L (55.6%), H-5→L+2 12.5%, H-6→L+1 (10.5%), H-5→L+1 (8.1%), H-6→L+2 (7.1%)
9	3.031	409.0 (490.8)	0.5964		H-2→L (37.8%), H-3→L+1 (16.6%), H-4→L+1 (16.2%), H-3→L+2 (14.6%), H-4→L+2 (9.0%)
10	3.035	408.6 (490.3)	0.4380		H-3→L (33.0%), H-2→L+1 (24.7%), H-4→L+2 (10.7%), H-4→L+1 (9.0%), H-2→L+2 (7.9%)

^a Only the TDDFT results of S_1 state and the S_n states with f larger than 0.01 among the first 10 S_n states were given. ^b The wavelengths multiplied by 1.2 were given in parentheses. ^c Oscillator strength. ^d Isovalue = 5×10^{-4} a.u. The electrons transfer from the blue regions to the purple regions during the excitation from S_0 state to S_n state. ^e The main orbital pairs involved in the excitation from S_0 state to S_n state. H = HOMO, L = LUMO. The transition contributions were provided in parentheses.

Table S7. The selected singlet-triplet spin-forbidden transitions of complex **1** in DMSO at PBE0-D3(BJ)/(Lanl2dz+6-31G(d,p)) level^a

No.	E(eV)	λ (nm)	EDD map ^b	Main transition ^c
1	1.738	713.2		H-3 \rightarrow L+1 (21.3%), H-2 \rightarrow L+1 (18.0%), H-3 \rightarrow L (17.8%), H-2 \rightarrow L (16.0%), H-3 \rightarrow L+2 (13.2%), H-2 \rightarrow L+2 (11.0%)
2	1.739	713.0		H-4 \rightarrow L+1 (34.9%), H-4 \rightarrow L (19.6%), H-2 \rightarrow L+1 (14.9%), H-2 \rightarrow L (9.4%), H-4 \rightarrow L+2 (6.4%), H-3 \rightarrow L+1 (6.3%)
3	1.739	713.0		H-3 \rightarrow L+2 (22.6%), H-4 \rightarrow L+2 (22.6%), H-2 \rightarrow L+2 (18.7%), H-4 \rightarrow L (13.5%), H-3 \rightarrow L (11.4%), H-2 \rightarrow L (8.5%)
4	2.457	504.6		H \rightarrow L (36.4%), H \rightarrow L+1 (13.6%), H-5 \rightarrow L (9.8%), H-1 \rightarrow L+1 (7.6%), H-1 \rightarrow L+2 (5.6%)

5	2.459	504.3		H→L+2 (37.0%), H→L+1 (14.1%), H-1→L (10.9%), H-5→L+2 (10.3%)
6	2.468	502.5		H-1→L+1 (23.8%), H-1→L (19.3%), H-1→L+2 (14.8%), H-6→L+1 (10.3%), H-6→L (7.8%), H-6→L+2 (6.6%)

^a Only the TDDFT results of the T_n states lower than S_1 state in energy were given. ^b Isovalue = 5×10^{-4} a.u. The electrons transfer from the blue regions to the purple regions during the excitation from S_0 state to T_n state. ^c The main orbital pairs involved in the excitation from S_0 state to S_n state. H = HOMO, L = LUMO. The transition contributions were provided in parentheses.

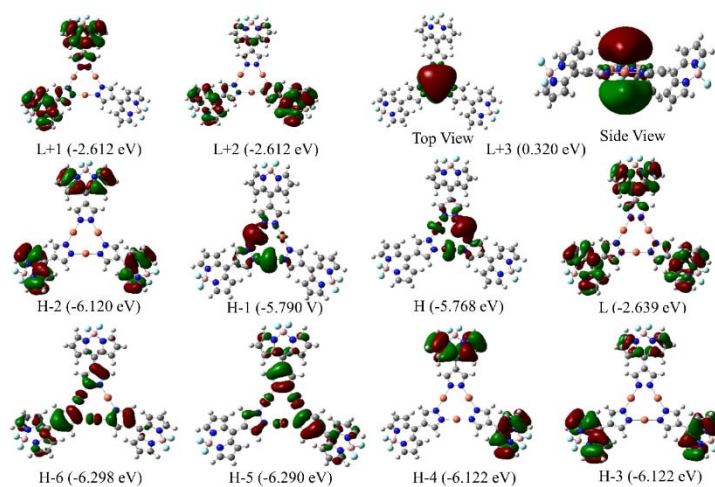


Fig. S41. The contours (Isovalue = 0.02) and energy levels (eV) of the selected molecular orbitals of complex **1**. H = HOMO, L = LUMO.

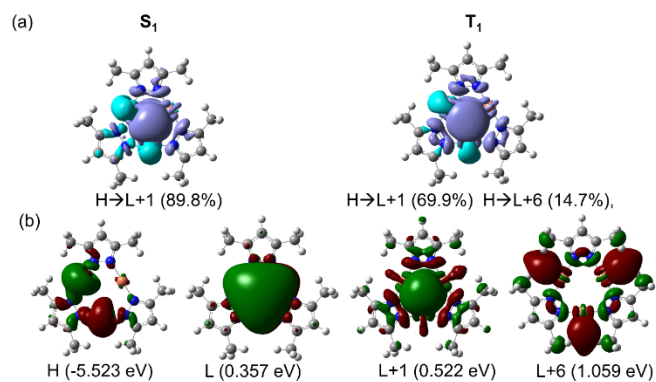


Fig. S42. (a) The EDD maps (Isovalue = 5×10^{-4} a.u.) of S_1 and T_1 states of complex **2** and their corresponding main transitions with transition contributions in parentheses. (b) The contours (Isovalue = 0.02) and energy levels of the molecular orbitals involved in the main transitions of S_1 and T_1 states of **2**. H = HOMO, L = LUMO.

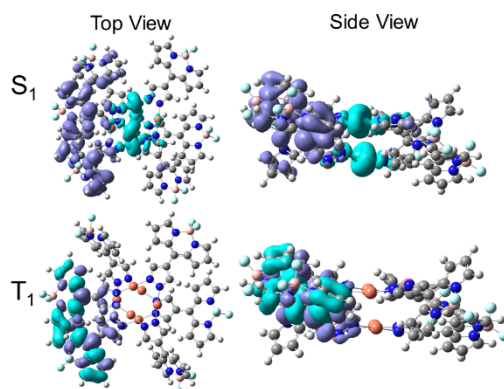


Fig. S43. The EDD maps of S_1 and T_1 states of the dimer of complex **1** based on the optimized ground-state geometry (isovalue = 5×10^{-4} a.u.)

3.14. Photocatalytic reaction

Photooxidation of DHN

The MeCN/MeOH (9:1, v/v) mixed solvent containing DHN (0.15 mM) and photosensitizer (3 μ M, 2 % mmol) were put into a borosilicate glass tube (50 mL) under an O₂ atmosphere. The solution was then irradiated using a 10 W LED light source of 370-780 nm.

Photooxidation of 4-formylphenylboronic acid

The MeCN/CH₂Cl₂ (5:1, v/v, 6 mL) mixed solvent containing 4-formylphenylboronic acid (14.9 mg, 0.1 mmol), N,N-diisopropylethylamine (DIPEA) (33 μ L, 0.2 mmol) and photosensitizer (20 μ M, 0.12 % mmol) were put into a borosilicate glass tube (50 mL) under an O₂ atmosphere. The solution was then irradiated using a 300 W Xenon light source of >420 nm.

Photooxidation of thioanisole

The EtOH/H₂O (1:1, v/v, 4mL) mixed solvent containing thioanisole (37.3 mg, 0.3 mmol) and photosensitizer (20 μ M, 0.03 % mmol) were put into a borosilicate glass tube (50 mL) under an air atmosphere. The solution was then irradiated using a 10 W LED light source of 370-780 nm.

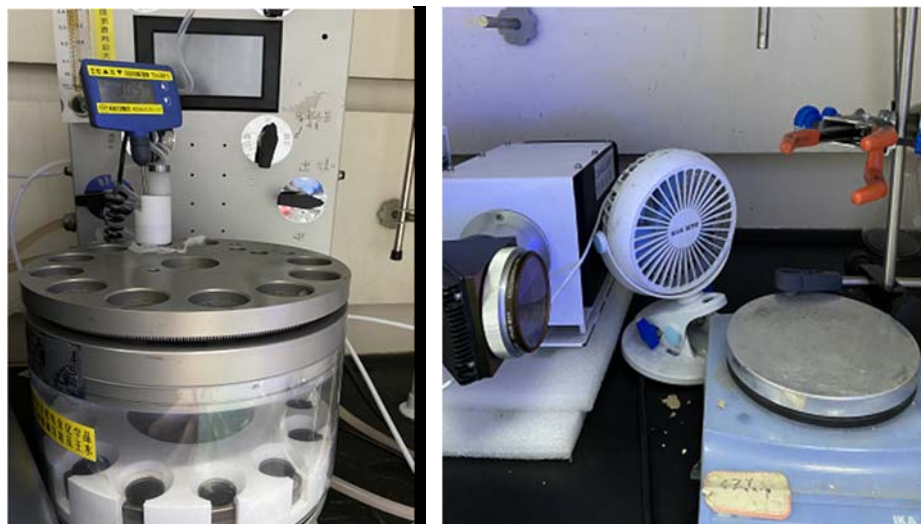
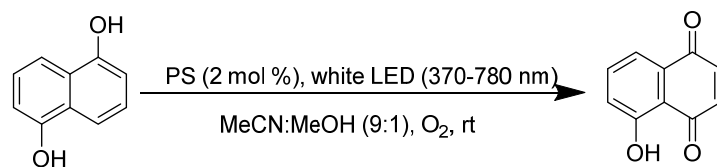
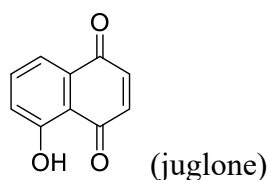


Fig. S44. The WP-TEC-1020HSL photooxidation reaction system with the white light LED (10 W) flow reactor is used to perform photooxidation reactions of DHN and thioanisole (left), photooxidation reaction of 4-formylphenylboronic acid was performed with a 300 W Xenon lamp (right).

Table S8. Optimization for photooxidation of DHN

Entry	catalyst	Solvent	Reaction time / h	Air or O ₂	yield ^a (%)
1	1	MeCN:MeOH (9:1)	2	O ₂	84
2	2	MeCN:MeOH (9:1)	2	O ₂	72
3	Ir(ppy)₃	MeCN:MeOH (9:1)	2	O ₂	81
4	1	MeCN:MeOH (9:1)	2	N ₂	40
5	HL	MeCN:MeOH (9:1)	2	N ₂	71
6	Cu(phen)₂BF₄²²	MeCN:MeOH (9:1)	2	N ₂	73

Reaction conditions: DHN (0.15 mM), PS (2 mol% vs. DHN); solvent (6 mL) and O atm. ^a The reported yield are estimated from the resulting absorbance at 427 nm and the molar extinction coefficient.²³



¹H NMR (400 MHz, 298 K, CDCl₃) δ 11.94 (s, 1H, OH), 7.66 (d, *J* = 7.5 Hz, 2H, CH_{Ph}), 7.32 (d, *J* = 7.5 Hz, 1H, CH_{Ph}), 6.98 (s, 2H, CH, CH_{Ph}) ppm. ¹³C NMR (100 MHz, 298 K, CDCl₃) δ 190.34, 184.33, 161.47, 139.63, 138.70, 136.63, 131.77, 124.55 119.22, 114.89 ppm.

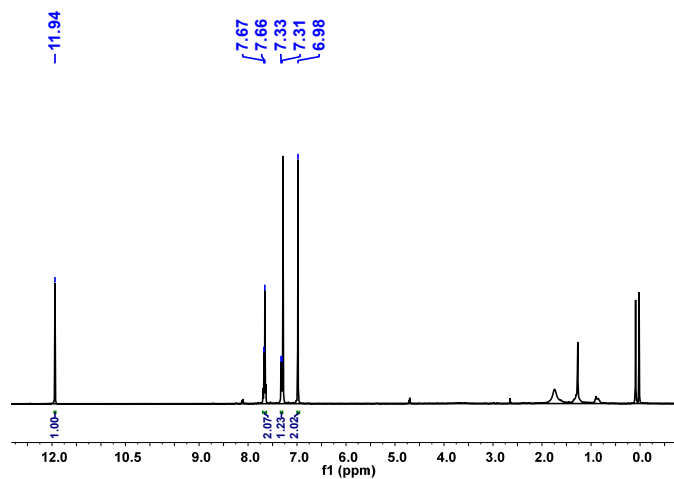


Fig. S45. ^1H NMR spectrum (400 MHz, 298 K, CDCl_3) of juglone.

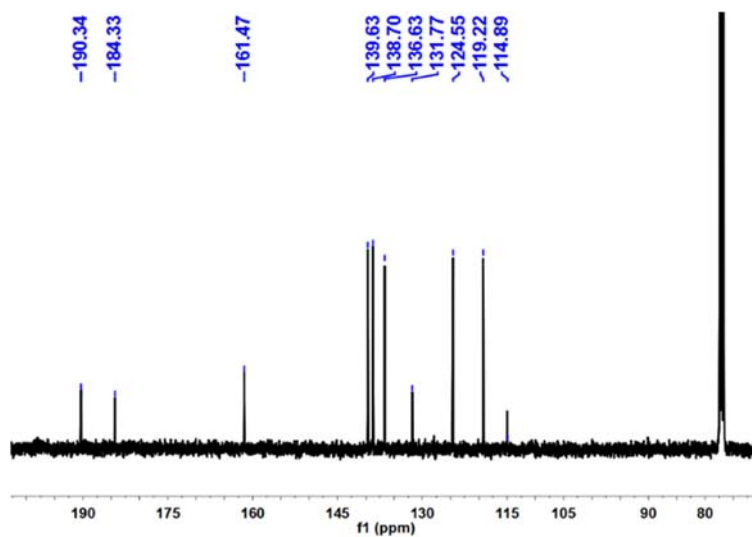


Fig. S46. ^{13}C NMR spectrum (100 MHz, 298 K, CDCl_3) of juglone.

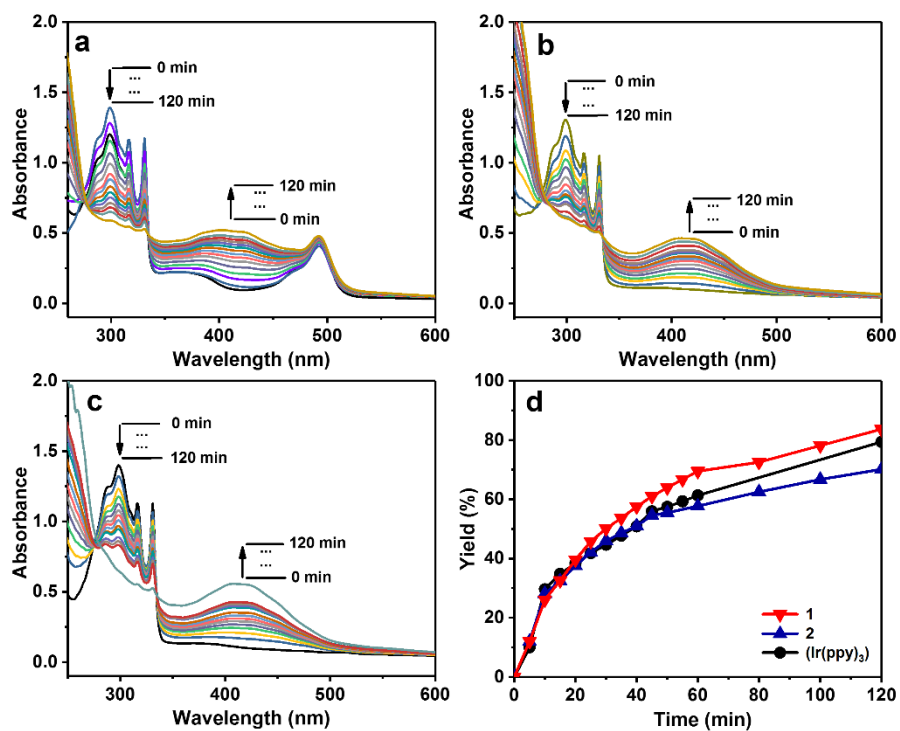


Fig. S47. Monitoring the change of the UV-vis absorption spectral for the photooxidation of DHN (0.15 mM) using complexes (a) **1**; (b) **2**; (c) Ir(ppy)_3 as singlet O_2 sensitizers; (d) The yields of juglone during 2 h irradiation with different PSs. $C_{\text{PS}} = 3 \mu\text{M}$ (2 mol % vs. DHN) in MeCN/MeOH (9/1, v/v). Irradiated with a 10 W white LED.

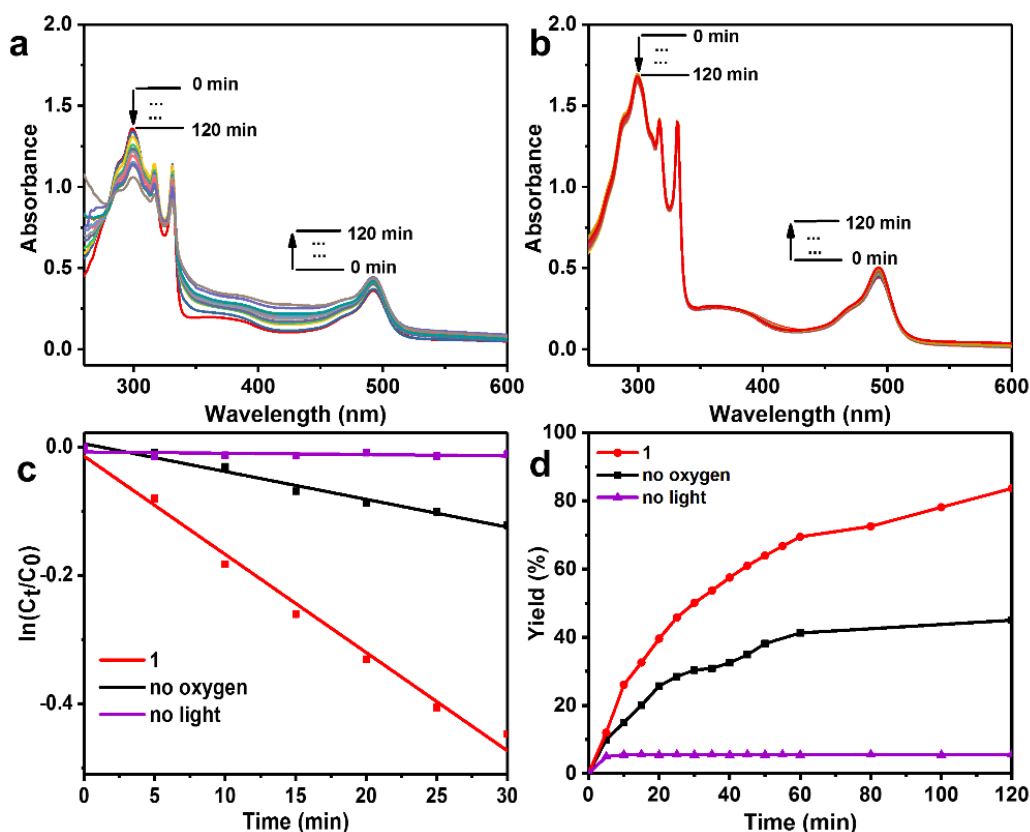


Fig. S48. Monitoring the change of the UV-vis absorption spectral change for the photooxidation of DHN (0.15 mM) using complexes **1** under different condition. (a) no oxygen; (b) no light; (c) Plot of $\ln(C_t/C_0)$ against irradiation time; (d) The yields of juglone during 2 h irradiation with complexes **1** under different condition. $C_{PS} = 3 \mu\text{M}$ (2 mol % vs. DHN) in MeCN/MeOH (9/1, v/v). Irradiated with a 10 W white LED.

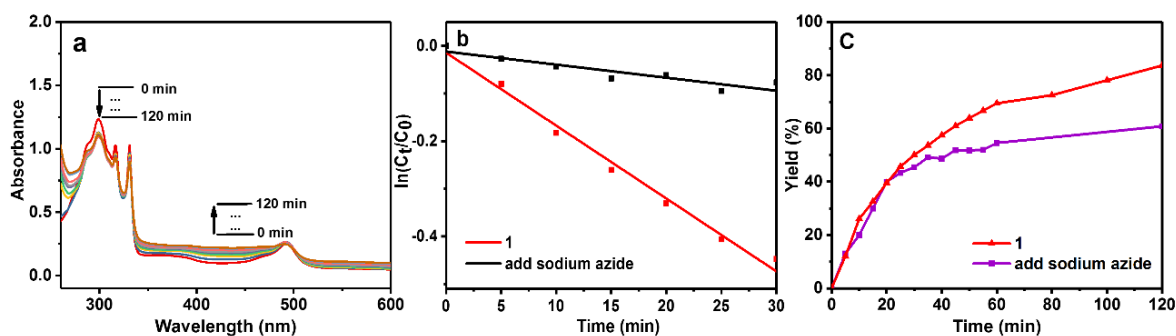
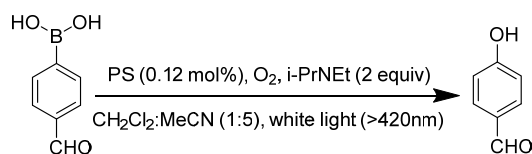
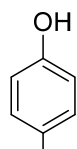


Fig. S49. (a) Monitoring the change of the UV-vis absorption spectral change for the photooxidation of DHN (0.15 mM) using complexes **1** with the quencher of $^1\text{O}_2$, sodium azide; (b) Plot of $\ln(C_t/C_0)$ against irradiation time; (c) The yields of juglone during 2 h irradiation with complexes **1** with sodium azide and no sodium azide. $C_{PS} = 3 \mu\text{M}$ (2 mol % vs. DHN) in MeCN/MeOH (9/1, v/v). Irradiated with a 10 W white LED.

Table S9. Optimization for photooxidation of 4-formylphenylboronic acid

Entry	catalyst	Solvent	PS loading / mol (%)	Yield (%)
1	1	CH ₂ Cl ₂ :MeCN (1:5)	1	97
2	1	CH ₂ Cl ₂ :MeCN (1:5)	0.12	95
3	2	CH ₂ Cl ₂ :MeCN (1:5)	0.12	5
4	Ir(ppy)₃	CH ₂ Cl ₂ :MeCN (1:5)	0.12	88
5	HL	CH ₂ Cl ₂ :MeCN (1:5)	0.12	50
6	Cu(phen)₂BF₄	CH ₂ Cl ₂ :MeCN (1:5)	0.12	7
7	Cu ₂ O	CH ₂ Cl ₂ :MeCN (1:5)	0.12	NR
8	CuI	CH ₂ Cl ₂ :MeCN (1:5)	0.12	NR
9	Cu(NO ₃) ₂ ·3H ₂ O	CH ₂ Cl ₂ :MeCN (1:5)	0.12	NR

Reaction conditions: 4-formylphenylboronic acid (0.1 mmol), PS (0.12 mol% vs. 4-formylphenylboronic acid); solvent (6 mL) and O₂ atm. ^a The reported yields are based on NMR analysis.



CHO (p-hydroxybenzaldehyde)

¹H NMR (400 MHz, 298 K, CDCl₃) δ 9.87 (s, 1H, CH), 7.84 (d, *J* = 8.6 Hz, 2H, CH_{Ph}), 7.02 (d, *J* = 8.6 Hz, 2H, CH_{Ph}) ppm. ¹³C NMR (100 MHz, 298 K, CDCl₃) δ 191.52, 162.18, 132.62, 129.53, 116.09 ppm.

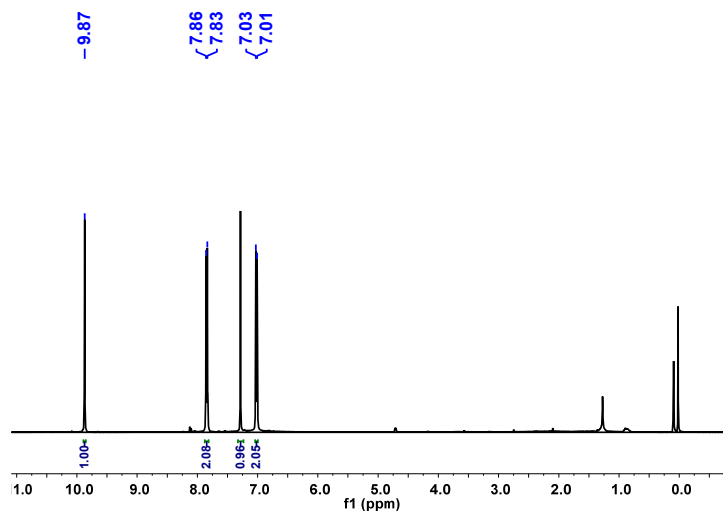


Fig. S50. ^1H NMR spectrum (400 MHz, 298 K, CDCl_3) of p-hydroxybenzaldehyde.

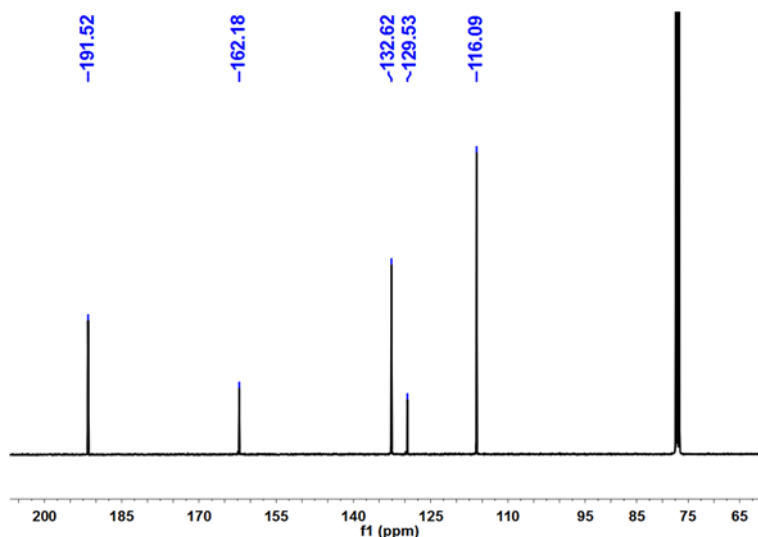


Fig. S51. ^{13}C NMR spectrum (100 MHz, 298 K, CDCl_3) of p-hydroxybenzaldehyde.

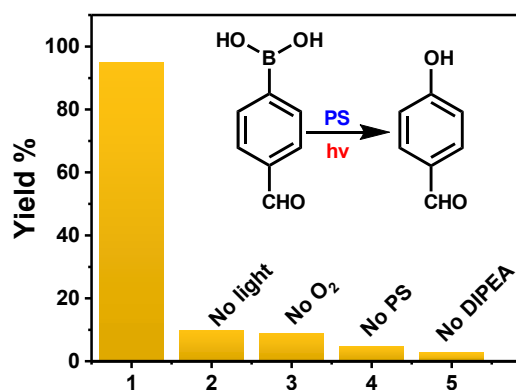
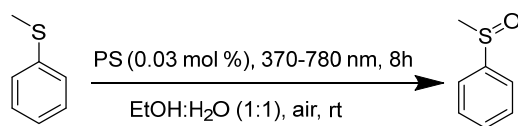
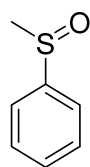


Fig. S52. Photocatalytic oxidative of 4-formylphenylboronic acid to p-hydroxybenzaldehyde at different conditions using **1** as photosensitizer.

Table S10. Optimization for photooxidation of thioanisole

Entry	catalyst	Solvent	Reaction time / h	PS loading / mol (%)	Air or O ₂	Yield (%)
1	1	MeOH	24	0.5	O ₂	26
2	1	EtOH:H ₂ O = 1:1	24	1	O ₂	99
3	1	EtOH:H ₂ O = 1:1	8	0.03	air	99
4	2	EtOH:H ₂ O = 1:1	8	0.03	air	3
6	Ir(ppy)₃	EtOH:H ₂ O = 1:1	8	0.03	air	7
7	HL	EtOH:H ₂ O = 1:1	8	0.03	air	99
8	Cu(phen)₂BF₄	EtOH:H ₂ O = 1:1	8	0.03	air	1
9	Cu ₂ O	EtOH:H ₂ O = 1:1	8	0.03	air	NR
10	CuI	EtOH:H ₂ O = 1:1	8	0.03	air	NR
11	Cu(NO ₃) ₂ ·3H ₂ O	EtOH:H ₂ O = 1:1	8	0.03	air	NR

Reaction conditions: thioanisole (0.1 mmol), PS (0.03 mol% vs. thioanisole); solvent (4 mL). ^a The reported yields are based on GCMS analysis.



(methyl phenyl sulfoxide)

¹H NMR (400 MHz, 298 K, CDCl₃) δ 7.64 (d, *J* = 1.8 Hz, 1H, CH_{Ph}), 7.62 (d, *J* = 1.4 Hz, 1H, CH_{Ph}), 7.56 – 7.51 (m, 1H, CH_{Ph}), 7.50 (s, 1H, CH_{Ph}), 7.47 (d, *J* = 6.9 Hz, 1H, CH_{Ph}), 2.71 (s, 3H, CH₃) ppm. ¹³C NMR (100 MHz, 298 K, CDCl₃) δ 145.56, 131.08, 129.38, 123.49, 43.92 ppm.

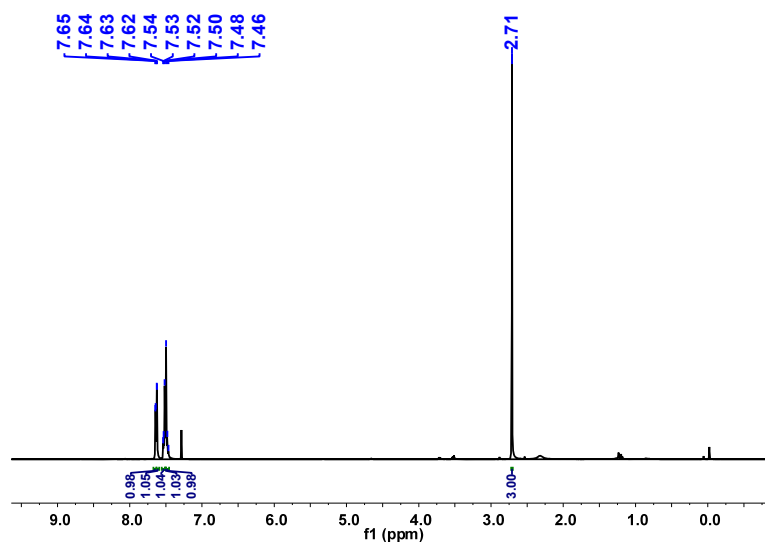


Fig. S53. ^1H NMR spectrum (400 MHz, 298 K, CDCl_3) of methyl phenyl sulfoxide.

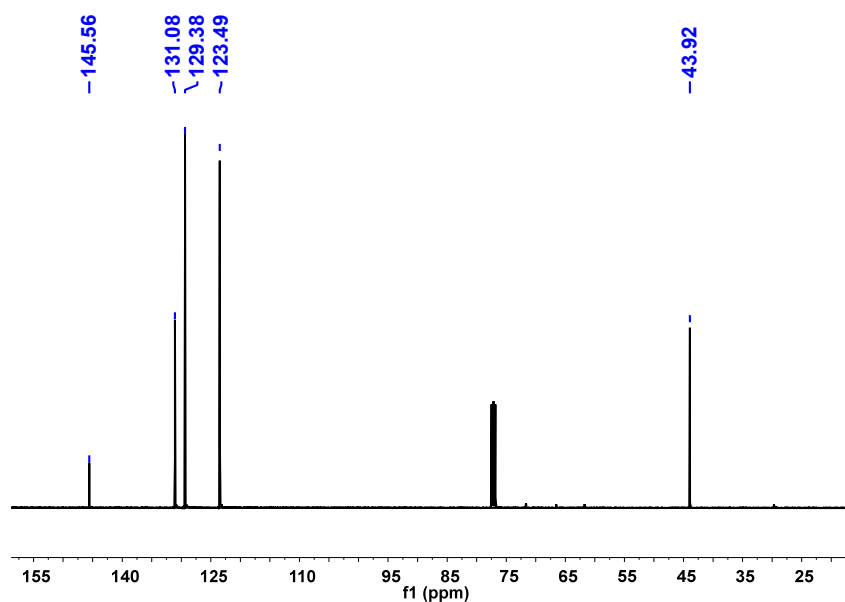
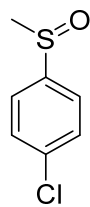


Fig. S54. ^{13}C NMR spectrum (100 MHz, 298 K, CDCl_3) of methyl phenyl sulfoxide.



(1-chloro-4-(methylsulfinyl)benzene)

^1H NMR (400 MHz, 298 K, CDCl_3) δ 7.64 – 7.58 (m, 2H, CH_{Ph}), 7.55 – 7.50 (m, 2H, CH_{Ph}), 2.74 (s, 3H, CH_3) ppm. ^{13}C NMR (100 MHz, 298 K, CDCl_3) δ 144.22 137.26, 129.66, 124.98, 44.06 ppm.

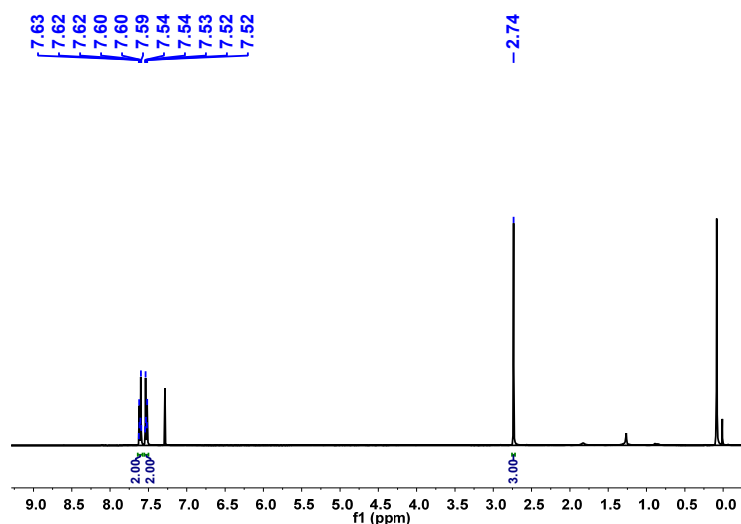


Fig. S55. ^1H NMR spectrum (400 MHz, 298 K, CDCl_3) of 1-chloro-4-(methylsulfinyl)benzene.

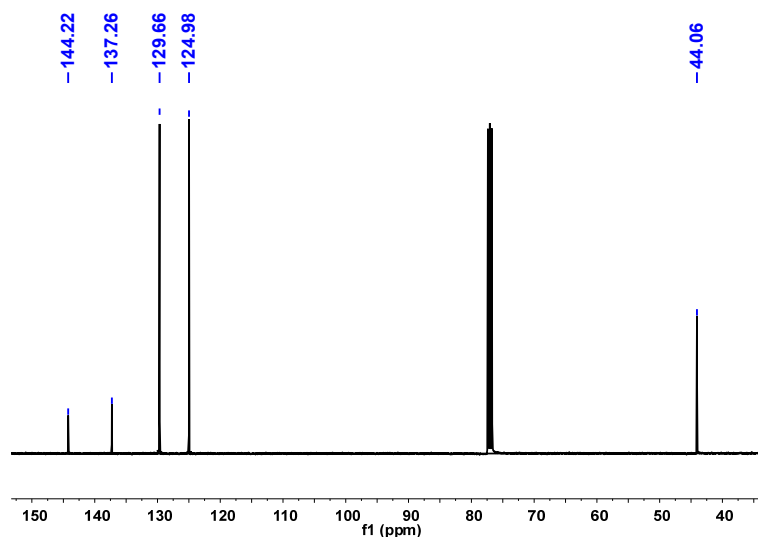
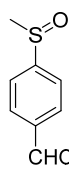


Fig. S56. ^{13}C NMR spectrum (100 MHz, 298 K, CDCl_3) of 1-chloro-4-(methylsulfinyl)benzene.



CHO (4-(methylsulfinyl)benzaldehyde)

^1H NMR (400 MHz, 298 K, CDCl_3) δ 10.07 (s, 1H, CH), 8.03 (d, $J = 8.0$ Hz, 2H, CH_{Ph}), 7.80 (d, $J = 8.0$ Hz, 2H, CH_{Ph}), 2.77 (s, 3H, CH_3) ppm. ^{13}C NMR (100 MHz, CDCl_3) δ 191.18, 152.47, 138.12, 130.41, 124.18, 43.79 ppm.

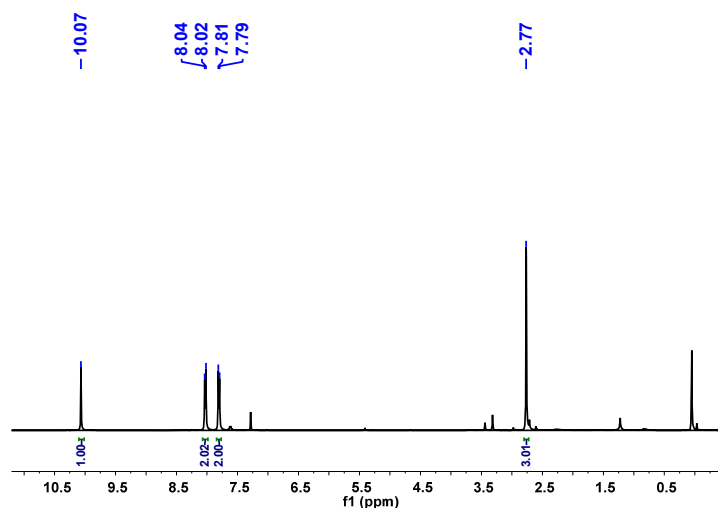


Fig. S57. ^1H NMR spectrum (400 MHz, 298 K, CDCl_3) of 4-(methylsulfinyl)benzaldehyde.

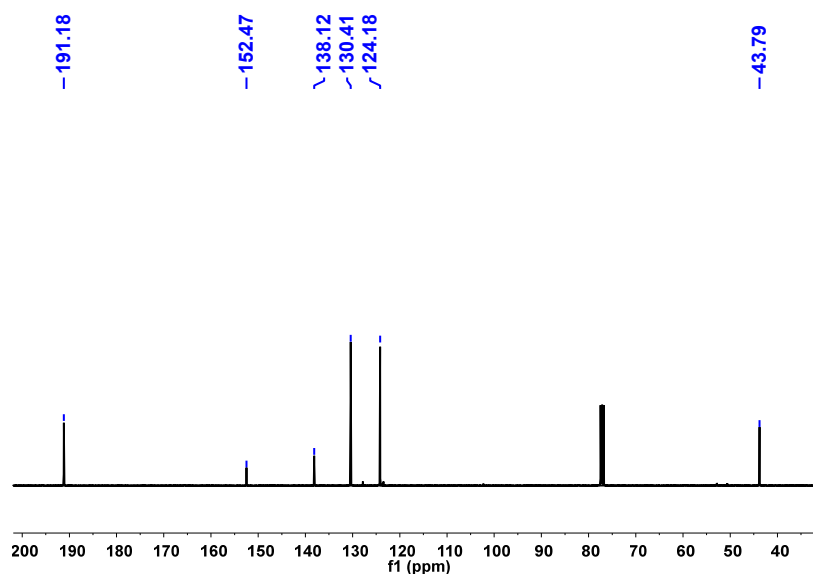
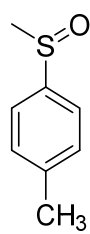


Fig. S58. ^{13}C NMR spectrum (100 MHz, 298 K, CDCl_3) of 4-(methylsulfinyl)benzaldehyde.



(1-methyl-4-(methylsulfinyl)benzene)

^1H NMR (400 MHz, 298 K, CDCl_3) δ 7.53 (d, J = 7.9 Hz, 2H, CH_{Ph}), 7.32 (d, J = 7.8 Hz, 2H, CH_{Ph}), 2.70 (s, 3H, CH_3), 2.41 (s, 3H, CH_3) ppm. ^{13}C NMR (100 MHz, 298 K, CDCl_3) δ 142.44, 141.52, 130.03, 123.55, 44.00, 21.40 ppm.

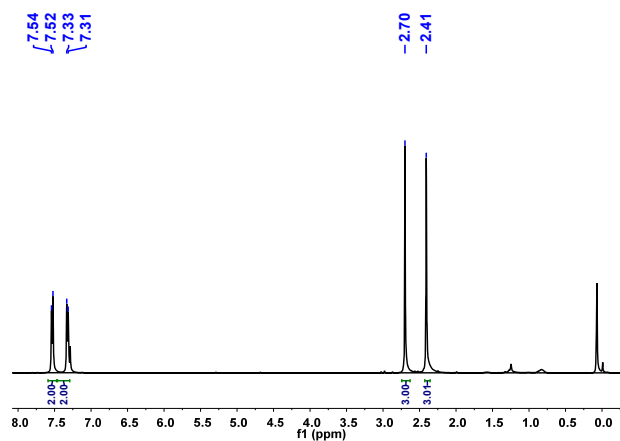


Fig. S59. ^1H NMR spectrum (400 MHz, 298 K, CDCl_3) of 1-methyl-4-(methylsulfinyl)benzene.

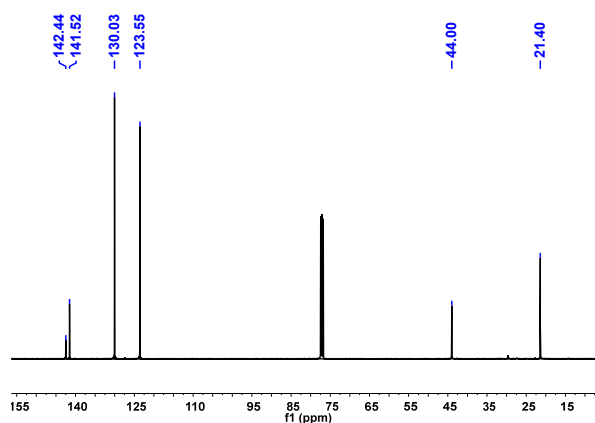


Fig. S60. ^{13}C NMR spectrum (100 MHz, 298 K, CDCl_3) of 1-methyl-4-(methylsulfinyl)benzene.

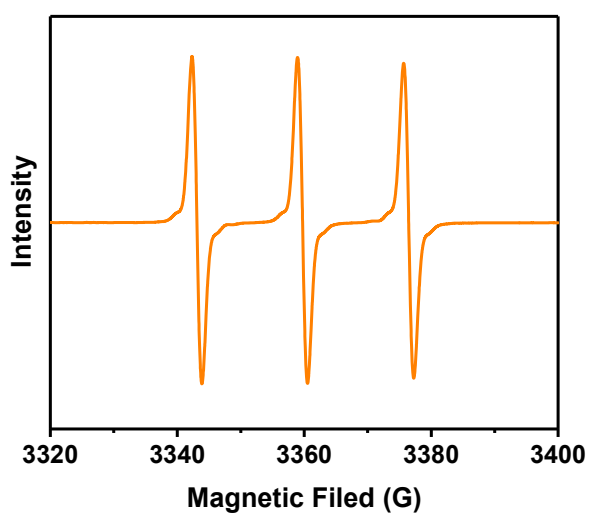


Fig. S61. EPR spectrum of **1** (0.001 mmol) in the presence of 0.3 mmol of TEMPO in mixture solution of EtOH and H_2O (1:1, v/v) under air.

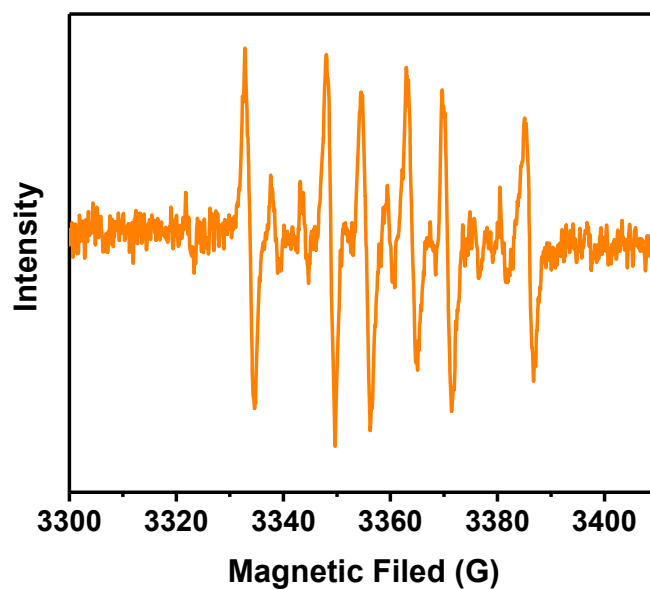


Fig. S62. EPR spectrum of **1** (0.001 mmol) in the presence of 0.3 mmol of DMPO in mixture solution of EtOH and H₂O (1:1, v/v) under air.

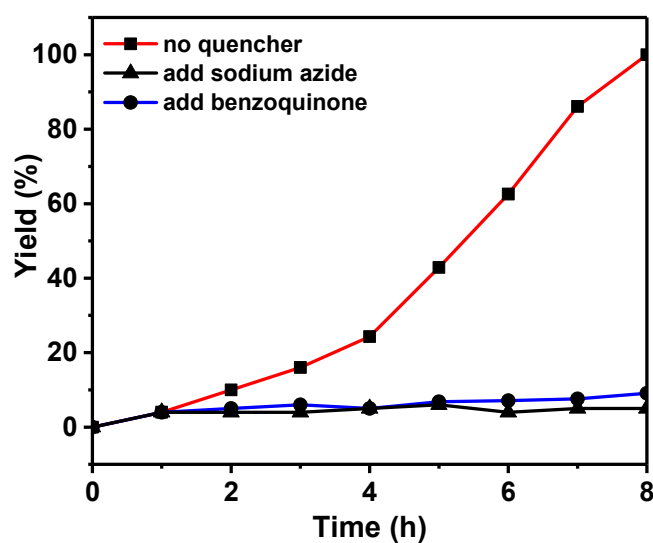


Fig. S63. The yields of methyl phenyl sulfoxide during 8 h irradiation with **1**, **1**+ BQ, and **1** + sodium azide in EtOH/H₂O (1/1, v/v). C_{PS}=20.0 μM (0.03 mol% vs substrates). Irradiated with a 10 W LED lamp.

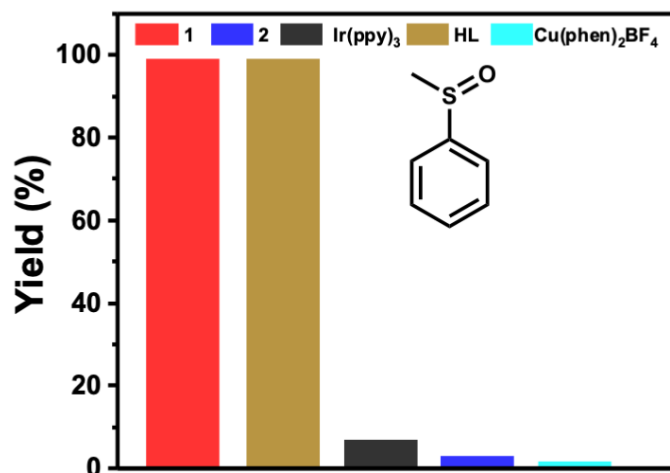
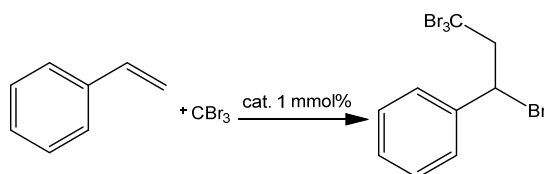


Fig. S64. Comparison of yields of methyl phenyl sulfoxide using different PSs including **1**, **2**, Ir(ppy)₃, HL and Cu(phen)₂BF₄.

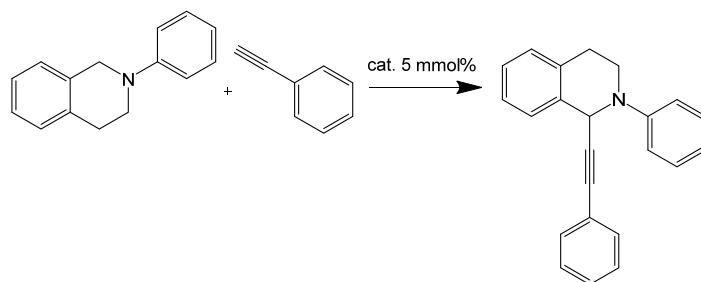
Table 11. Optimization of reaction conditions for the synthesis of (1,3,3,3-tetrabromopropyl)benzene^a



Entry	catalyst	Solvent	Catalyst loading / mol (%)	Yield (%) ^b
1	HL	CH ₂ Cl ₂	1	18
2	1	CH ₂ Cl ₂	1	55
3	2	CH ₂ Cl ₂	1	49
4	Cu(phen)₂BF₄	CH ₂ Cl ₂	1	64

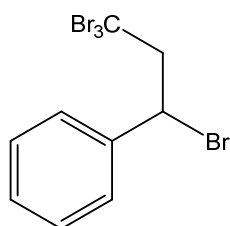
^a Model reaction conditions: alkene (0.2 mmol), carbon tetrabromide (0.2 mmol) in dichloromethane (1.0 mL) under irradiation of 90 W white LED in N₂ atmosphere at rt for 24 h. ^b The yield of (1,3,3,3-tetrabromopropyl)benzene was determined by ¹H NMR with 1,1,2,2-tetrachloroethane as internal standard.

Table 12. Optimization of reaction conditions for the synthesis of 2-phenyl-1-(phenylethynyl)-1,2,3,4-tetrahydroisoquinoline^a



Entry	catalyst	Solvent	Catalyst loading / mol (%)	Yield (%) ^b
1	HL	MeCN	5	2
2	1	MeCN	5	43
3	2	MeCN	5	4
4	Cu(phen)₂BF₄	MeCN	5	39

^aModel reaction conditions: 2-phenyl-1,2,3,4-tetrahydroisoquinoline (0.1 mmol), ethynylbenzene (0.1 mmol) in acetonitrile (1.0 mL) under irradiation of 10 W white LED in air at rt for 12 h. ^bThe yield of 2-phenyl-1-(phenylethynyl)-1,2,3,4-tetrahydroisoquinoline was determined by ¹H NMR with 1,1,2,2-tetrachloroethane as internal standard.



(1,3,3,3-tetrabromopropyl)benzene)

¹H NMR (400 MHz, 298 K, CDCl₃) δ 7.50 (d, J = 7.0 Hz, 2H, CH_{Ph}), 7.37 (t, J = 7.3 Hz, 2H, CH_{Ph}), 7.31 (t, J = 7.2 Hz, 2H, CH_{Ph}), 5.34 (dd, J = 7.7 Hz, 4.1 Hz, 1H, CH), 4.13 (dd, J = 15.5 Hz, 4.1 Hz, 1H, CH₂), 4.06 (dd, J = 15.6 Hz, 7.7 Hz, 1H, CH₂) ppm. ¹³C NMR (100 MHz, 298 K, CDCl₃) δ 140.79, 129.22, 128.94, 128.18, 127.69, 66.45, 50.09, 35.07 ppm.

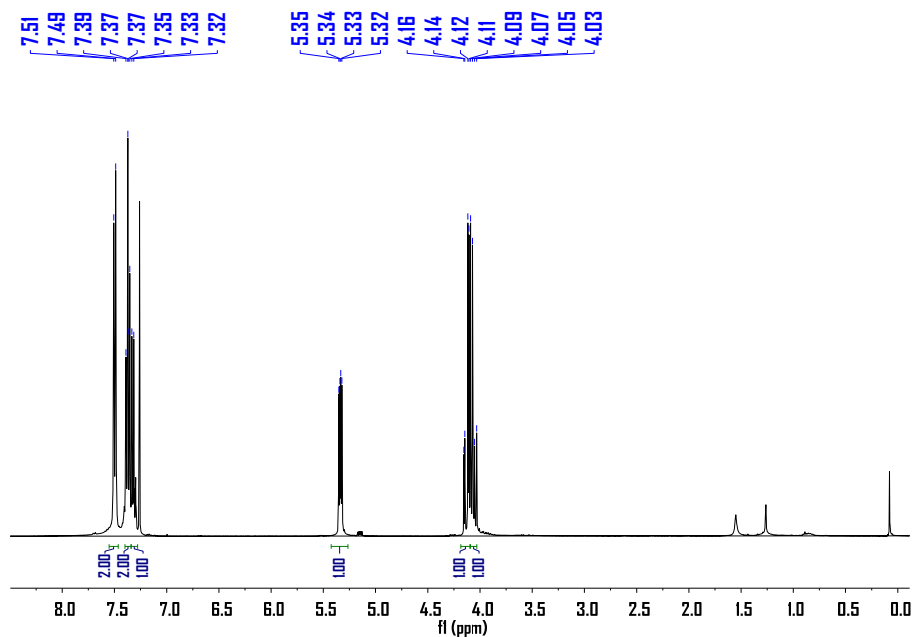


Fig. S65. ^1H NMR spectrum (400 MHz, 298 K, CDCl_3) of 1,3,3,3-tetrabromopropylbenzene.

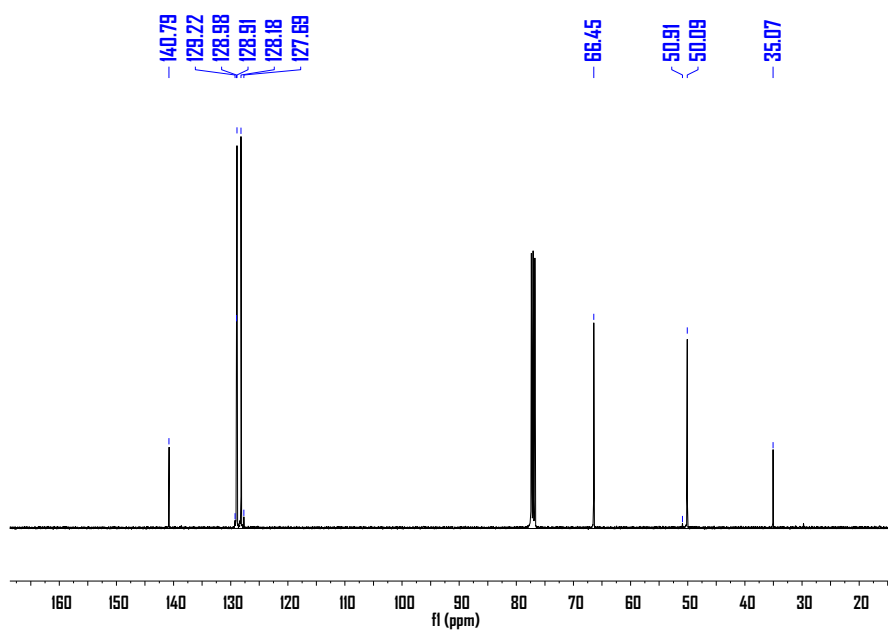
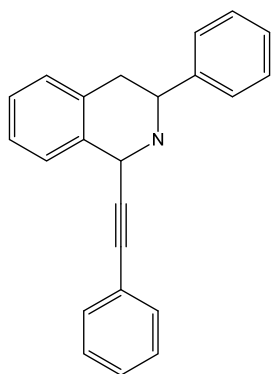


Fig. S66. ^{13}C NMR spectrum (100 MHz, 298 K, CDCl_3) of 1,3,3,3-tetrabromopropylbenzene.



(2-phenyl-1-(phenylethynyl)-1,2,3,4-tetrahydroisoquinoline)

^1H NMR (400 MHz, 298 K, CDCl_3) δ 7.43 – 7.27 (m, 6H, CH_{Ph}), 7.24 (m, 5H, CH_{Ph}), 7.15 (d, $J = 8.2$ Hz, 2H, CH_{Ph}), 6.91 (t, $J = 7.2$ Hz, 1H, CH_{Ph}), 5.66 (s, 1H, CH), 3.77–3.63 (m, 2H, CH_2), 3.18 (dd, $J = 14.2, 8.1$ Hz, 1H, CH_2), 3.05 – 2.95 (m, 1H, CH_2) ppm. ^{13}C NMR (100 MHz, 298 K, CDCl_3) δ 149.40, 135.29, 134.33, 131.75, 129.16, 128.94, 128.09, 128.06, 127.44, 127.27, 126.31, 122.96, 116.84, 88.43, 84.92, 77.25, 52.45, 43.57, 28.87 ppm.

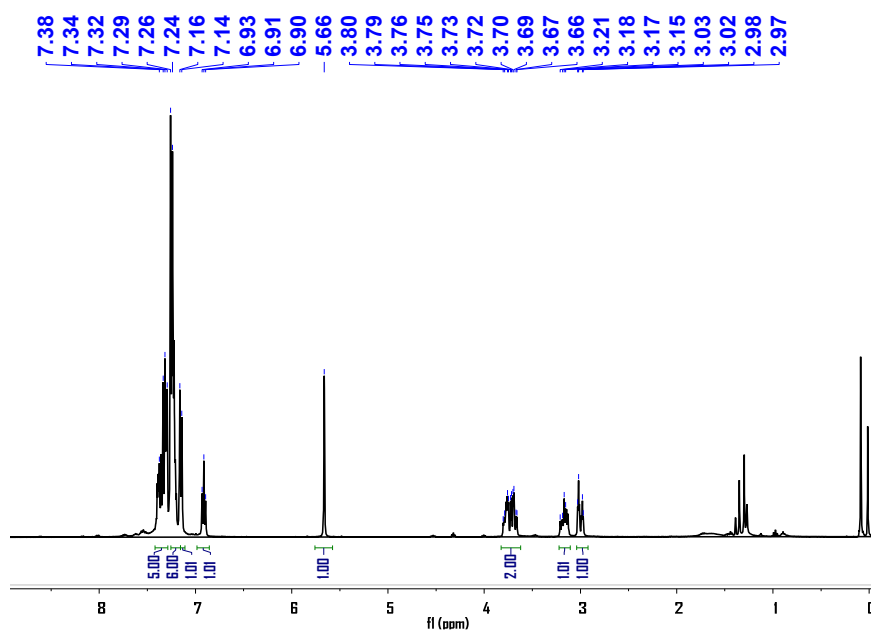


Fig. S67. ^1H NMR spectrum (400 MHz, 298 K, CDCl_3) of 2-phenyl-1-(phenylethynyl)-1,2,3,4-tetrahydroisoquinoline.

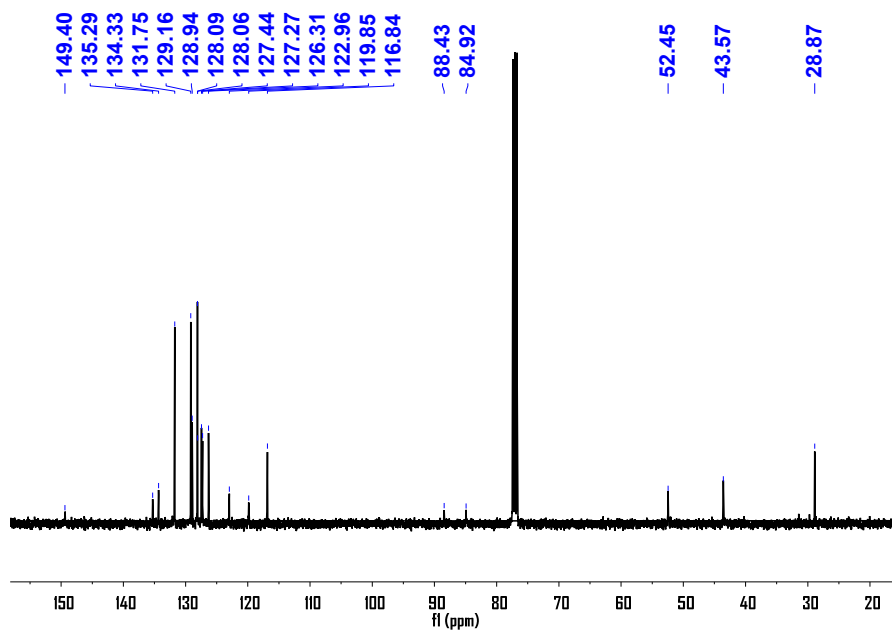


Fig. S68. ^{13}C NMR spectrum (100 MHz, 298 K, CDCl_3) of 2-phenyl-1-(phenylethynyl)-1,2,3,4-tetrahydroisoquinoline.

3.15. Photooxidation stability test

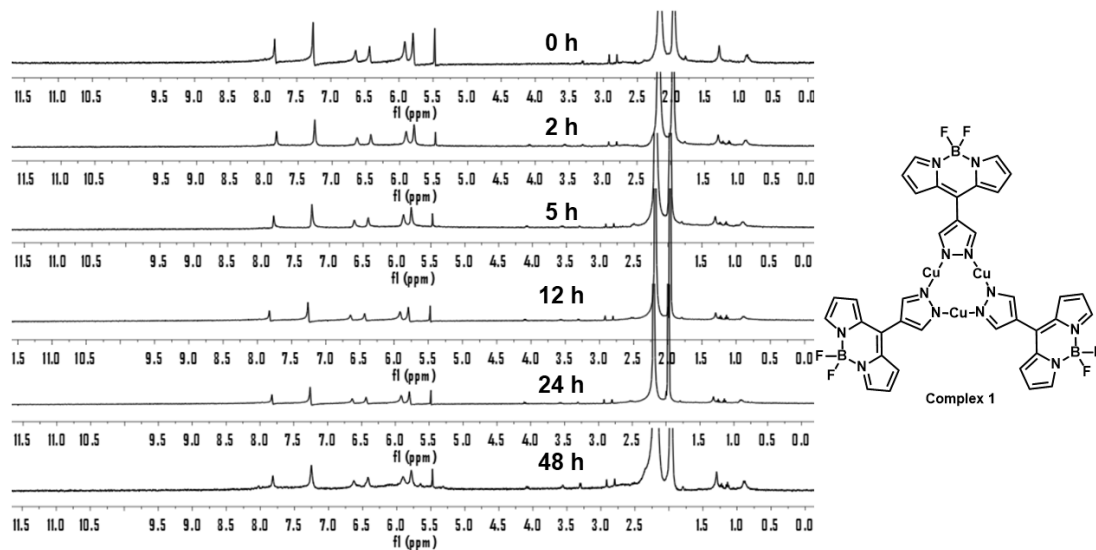


Fig. S69. ^1H NMR spectra (400 MHz, 298 K, CD_3CN) of complex 1 under 10 W white light irradiation.

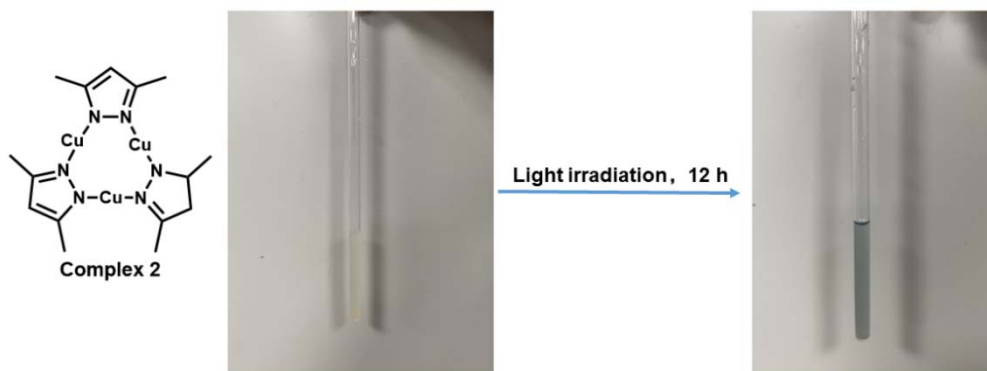


Fig. S70. The pictures of complex 2 before light irradiation and after 10 W white light irradiation for 12 h.

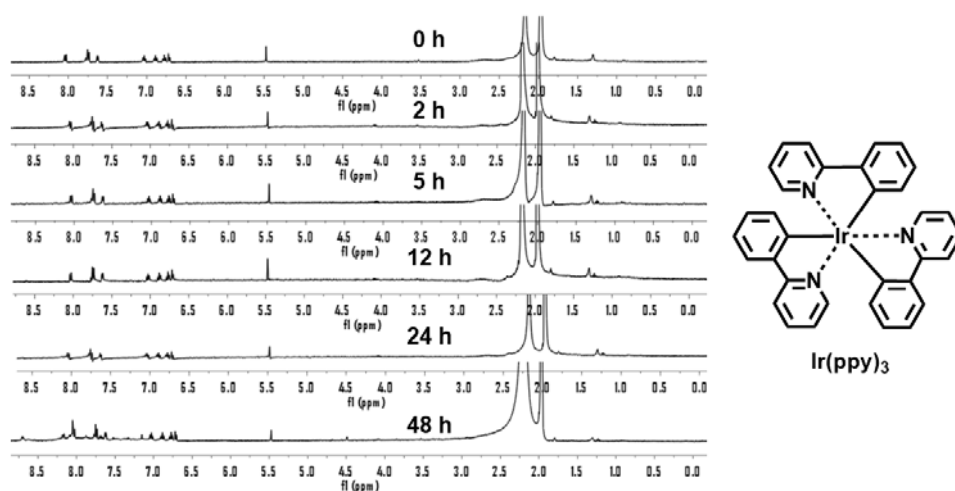


Fig. S71. ¹H NMR spectra (400 MHz, 298 K, CD₃CN) of Ir(ppy)₃ under 10 W white light irradiation.

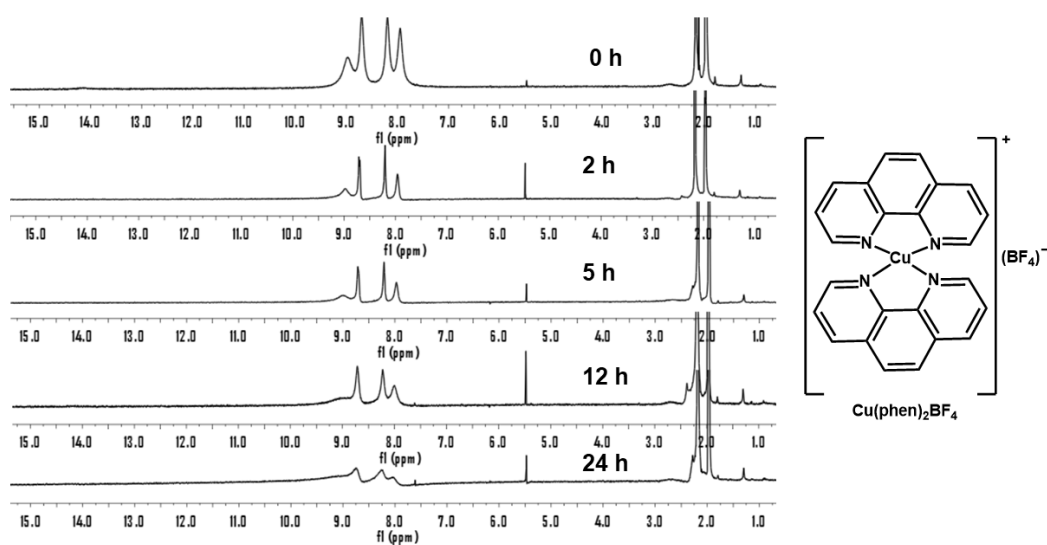


Fig. S72. ¹H NMR spectra (400 MHz, 298 K, CD₃CN) of Cu(phen)₂BF₄ under 10 W white light irradiation.

References

- 1 R. Liang, S.-S. Sun, G. Huang and M.-D. Li, Unveiling the Photophysical and Photochemical Reaction Process of Naproxen via Ultrafast Femtosecond to Nanosecond Laser Flash Photolysis, *Chem. Res. Toxicol.*, 2019, **32**, 613-620.
- 2 Z. Deng, S. Sun, M. Zhou, G. Huang, J. Pang, L. Dang and M.-D. Li, Revealing Ultrafast Energy Dissipation Pathway of Nanocrystalline Sunscreens Oxybenzone and Dioxybenzone, *J. Phys. Chem. Lett.*, 2019, **10**, 6499-6503.
- 3 T. V. Goud, A. Tutar and J.-F. Biellmann, Synthesis of 8-heteroatom-substituted 4,4-difluoro-4-bora-3a,4a-diaza-s-indacene dyes (BODIPY), *Tetrahedron*, 2006, **62**, 5084-5091.
- 4 X.-L. Lv, K. Wang, B. Wang, J. Su, X. Zou, Y. Xie, J.-R. Li and H.-C. Zhou, A Base-Resistant Metalloporphyrin Metal–Organic Framework for C–H Bond Halogenation, *J. Am. Chem. Soc.*, 2017, **139**, 211-217.
- 5 M. K. Ehlert, S. J. Rettig, A. Storr, R. C. Thompson and J. Trotter, Synthesis and X-ray crystal structure of the 3,5-dimethylpyrazolato copper(I) trimer, [Cu(pz'')]₃, *Can. J. Chem.*, 1990, **68**, 1444-1449.
- 6 H. V. R. Dias, H. V. K. Diyabalanage, M. G. Eldabaja, O. Elbjeirami, M. A. Rawashdeh-Omary and M. A. Omary, Brightly Phosphorescent Trinuclear Copper(I) Complexes of Pyrazolates: Substituent Effects on the Supramolecular Structure and Photophysics, *J. Am. Chem. Soc.*, 2005, **127**, 7489-7501.
- 7 G. Sheldrick, A short history of SHELX, *Acta Cryst. A*, 2008, **64**, 112-122.
- 8 O. V. Dolomanov, L. J. Bourhis, R. J. Gildea, J. A. K. Howard and H. Puschmann, OLEX2: a complete structure solution, refinement and analysis program, *J. Appl. Cryst.*, 2009, **42**, 339-341.
- 9 M. J. Frisch, G. W. Trucks, H. B. Schlegel, G. E. Scuseria, M. A. Robb, J. R. Cheeseman, G. Scalmani, V. Barone, B. Mennucci, G. A. Petersson, H. Nakatsuji, M. Caricato, X. Li, H. P. Hratchian, A. F. Izmaylov, J. Bloino, G. Zheng, J. L. Sonnenberg, M. Hada, M. Ehara, K. Toyota, R. Fukuda, J. Hasegawa, M. Ishida, T. Nakajima, Y. Honda, O. Kitao, H. Nakai, T. Vreven, Jr. J. A. Montgomery, J. E.

- Peralta, F. Ogliaro, M. Bearpark, J. J. Heyd, E. Brothers, K. N. Kudin, V. N. Staroverov, R. Kobayashi, J. Normand, K. Raghavachari, A. Rendell, J. C. Burant, S. S. Iyengar, J. Tomasi, M. Cossi, N. Rega, J. M. Millam, M. Klene, J. E. Knox, J.B. Cross, V. Bakken, C. Adamo, J. Jaramillo, R. Gomperts, R. E. Stratmann, O. Yazyev, A. J. Austin, R. Cammi, C. Pomelli, J. Ochterski, R. L. Martin, K. Morokuma, V. G. Zakrzewski, G. A. Voth, P. Salvador, J. J. Dannenberg, S. Dapprich, A. D. Daniels, O. Farkas, J. B. Foresman, J. V. Ortiz, J. Cioslowski and D. J. Fox, Gaussian 09 (Revision E.01), Gaussian, Inc., Wallingford, CT, 2013.
- 10 J. P. Perdew, K. Burke and M. Ernzerhof, Generalized Gradient Approximation Made Simple, *Phys. Rev. Lett.*, 1996, **77**, 3865-3868.
 - 11 J. P. Perdew, K. Burke and M. Ernzerhof, Generalized Gradient Approximation Made Simple [Phys. Rev. Lett. 77, 3865 (1996)], *Phys. Rev. Lett.*, 1997, **78**, 1396.
 - 12 S. Grimme, J. Antony, S. Ehrlich and H. Krieg, A consistent and accurate ab initio parametrization of density functional dispersion correction (DFT-D) for the 94 elements H-Pu, *J. Chem. Phys.*, 2010, **132**, 154104.
 - 13 S. Grimme, S. Ehrlich and L. Goerigk, Effect of the damping function in dispersion corrected density functional theory, *J. Comput. Chem.*, 2011, **32**, 1456–1465.
 - 14 T. H. Dunning, Jr., and P. J. Hay, In Modern Theoretical Chemistry; Schaefer, H. F., III., Ed.; Plenum: New York, 1976, Vol. 3, pp 1–28.
 - 15 P. J. Hay and W. R. Wadt, *Ab initio* effective core potentials for molecular calculations. Potentials for the transition metal atoms Sc to Hg, *J. Chem. Phys.*, 1985, **82**, 270.
 - 16 W. R. Wadt and P. J. Hay, *Ab initio* effective core potentials for molecular calculations. Potentials for main group elements Na to Bi, *J. Chem. Phys.*, 1985, **82**, 284.
 - 17 P. J. Hay and W. R. Wadt, *Ab initio* effective core potentials for molecular calculations. Potentials for K to Au including the outermost core orbitals, *J. Chem. Phys.*, 1985, **82**, 299.
 - 18 P. C. Hariharan, and J. A. Pople, Accuracy of AH_n equilibrium Geometries by

- Single Determinant Molecular Orbital Theory, *Mol. Phys.*, 1974, **27**, 209.
- 19 A. V. Marenich, C. J. Cramer and D. G. Truhlar, Universal Solvation Model Based on Solute Electron Density and on a Continuum Model of the Solvent Defined by the Bulk Dielectric Constant and Atomic Surface Tensions. *J. Phys. Chem. B*, 2009, **113**, 6378-6396.
 - 20 T. Lu and F. Chen, Multiwfn: A multifunctional wavefunction analyzer, *J. Comput. Chem.*, 2012, **33**, 580-592.
 - 21 Z. Liu, T. Lu, Q. Chen, An sp-hybridized all-carboatomic ring, cyclo[18]carbon: Electronic structure, electronic spectrum, and optical nonlinearity, *Carbon*, 2020, **165**, 461-467.
 - 22 H. Fuwa, Total synthesis of tetrahydropyran-containing natural products exploiting intramolecular oxa-conjugate cyclization, *Heterocycles*, 2012, **85**, 1255-1298.
 - 23 S.-Y. Takizawa, R. Aboshi and S. Murata, Photooxidation of 1,5-dihydroxynaphthalene with iridium complexes as singlet oxygen sensitizers, *Photochem. Photobiol. Sci.*, 2011, **10**, 895-903.